

Supporting Information

Pyridine Dicarbanion-bonded Ag₁₃ Organometallic Nanoclusters: Synthesis and On-surface Oxidative Coupling Reaction

Cui-Cui Li, Siqi Zhang, Jian Tang, Ruijun Jian, Yu Xia and Liang Zhao*

Key Laboratory of Bioorganic Phosphorus Chemistry & Chemical Biology (Ministry of Education), Department of Chemistry, Tsinghua University, Beijing 100084, China

E-mail: zhaolchem@mail.tsinghua.edu.cn; Phone: +86-10-62786635.

Table of Contents

1	General Information	S3
2	X-ray Crystallographic Studies	S3
3	Supporting Figures	S6
4	Supporting Tables	S27
5	References	S28

Experimental Procedures

1. General Information

Computational details

Theoretical calculations of ${}^{\text{Me}}\text{PyAg}_5$, ${}^{\text{Me}}\text{PyAg}_{13}$, ${}^{\text{Ph}}\text{PyAg}_{13}$ -based model clusters were performed using the Gaussian 09 program¹ and ORCA ab initio.² The TZVP basis sets³ are used for all atoms for geometry optimizations of ${}^{\text{Me}}\text{PyAg}_{13}$ and ${}^{\text{Ph}}\text{PyAg}_{13}$ with the functional of BP86.⁴ Solvation effects of acetone were accounted by using the SMD⁵ continuum solvation model. The scaling method⁶ was used to calculate the NMR of ${}^{\text{Me}}\text{PyAg}_{13}$ and ${}^{\text{Ph}}\text{PyAg}_{13}$ with the functional of b3lyp⁷ and 6-31G(d)⁸ (C, H, N atoms) & SDD⁹ (Ag atoms) basis set. Data for orbital composition analysis with Mulliken partition are from Gaussian 09 calculations and processed with Multiwfn software.¹⁰ Initial structure for molecular orbital analysis of ${}^{\text{Me}}\text{PyAg}_5$ was built up on the basis of single crystal structure with the functional of b3lyp⁷ and 6-31G(d)⁸ (C, H, N, O, S, F atoms) & LanL2DZ¹¹ (Ag atoms) basis sets. The bond order, IGMH analysis and AIM analysis of ${}^{\text{Me}}\text{PyAg}_{13}$ were realized by Multiwfn and VMD¹² software.

DOSY measurement

DOSY experiments were carried out on a Bruker Avance 600 MHz instrument using a 5mm TXI HC/N Z-GRD probe. 2D sequence for diffusion measurements were conducted using stimulated echo and LED with 2 spoil gradients. All ${}^1\text{H}$ -DOSY spectra were recorded at 298 K with 50 ms diffusion delay, 16 squared increments for gradient levels and 32 transients. Gradient strength was set as 50 G/cm. Molecular sizes of ${}^{\text{Me}}\text{PyAg}_{13}$ in d_6 -Acetone were calculated according to the Einstein-Stokes equation:

$$D = k_B T / 6\pi\eta r$$

T : temperature (K); η : viscosity constant of acetone = 3.16×10^{-4} Pa·s; kB : Boltzmann's constant; D : diffusion coefficient; r : radius of the spherical particle.

2. X-ray Crystallographic Studies

Single-crystal X-ray data for silver cluster complexes were collected with Mo-K α radiation ($\lambda = 0.71073$ Å) on a Rigaku Saturn 724/724 + CCD diffractometer with frames of oscillation range 0.5° . The selected crystal was mounted onto a nylon loop by polyisobutene and enveloped in a low-temperature stream of dry nitrogen gas during data collection. The absorption corrections were applied using multi-scan methods. All structures were solved by direct methods, and non-hydrogen atoms were located from difference Fourier maps. Non-hydrogen atoms were subjected to anisotropic refinement by full-matrix least-squares on F^2 using the SHELXTL program¹³ unless otherwise noted. The diffused electron density in the remaining void was treated by SQUEEZE program on the PLATON platform.¹⁴ All figures were drawn by using X-seed¹⁵ and Diamond program.

Crystal data for ${}^{\text{Me}}\text{PyAg}_5$ ($[\text{Ag}_5(\text{C}_6\text{NH}_5)(\text{Py}[8])](\text{CF}_3\text{SO}_3)_3$) (CCDC-1996369): $C_{57}\text{H}_{53}\text{Ag}_5\text{F}_9\text{N}_{17}\text{O}_9\text{S}_3$, $M = 1925.68$, monoclinic, space group C2/c (No. 15), $a = 25.7535(5)$ Å, $b = 24.5293(6)$ Å, $c = 24.9163(4)$ Å, $\beta = 91.174(2)^\circ$, $V = 15736.7(6)$ Å³, $Z = 8$, $T = 173$ K, $D_c = 1.627$ g cm⁻³. The structure, refined on F^2 , converged for 14876 unique reflections ($R_{\text{int}} = 0.034$) and 11488 observed reflections with $I > 2\sigma(I)$ to give $R_1 = 0.0727$ and $wR_2 = 0.2176$ and a goodness-of-fit = 1.041. The silver atom Ag04 was disordered at two positions with a refined site

occupancy ratio of 0.95:0.05. The SQUEEZE procedure of PLATON was used in the processing of **MePyAg₅**. In the checkCIF report of **MePyAg₅**, there are two B alerts of “High ‘MainMol’ Ueq as Compared to Neighbors of O029” and “Low ‘MainMol’ Ueq as Compared to Neighbors of S007”, which can be ascribed to the disorders of triflate anions in the structure of **MePyAg₅**.

Crystal data for *n*-PrPyAg₅ ([Ag₅(C₈NH₉)(Py[8])](CF₃SO₃)₃) (CCDC-2062353): C₅₉H₅₇Ag₅F₉N₁₇O₉S₃, $M = 3909.50$, triclinic, space group P-1 (No. 2), $a = 14.8014(4)$ Å, $b = 22.3158(5)$ Å, $c = 24.8300(6)$ Å, $\alpha = 84.932(2)^\circ$, $\beta = 76.949(2)^\circ$, $\gamma = 73.121(2)^\circ$, $V = 7643.2(3)$ Å³, $Z = 4$, $T = 100$ K, $D_c = 1.699$ g cm⁻³. The structure, refined on F^2 , converged for 27744 unique reflections ($R_{\text{int}} = 0.0571$) and 19864 observed reflections with $I > 2\sigma(I)$ to give $R_1 = 0.0591$ and $wR_2 = 0.1229$ and a goodness-of-fit = 1.020. The SQUEEZE procedure of PLATON was used in the processing of ***n*-PrPyAg₅**. The three B alerts in the checkCIF report of ***n*-PrPyAg₅** may be ascribed to the disorders of triflate anions in the structure of ***n*-PrPyAg₅**.

Crystal data for PhPyAg₅ ([Ag₅(C₁₁NH₇)(Py[8])](CF₃SO₃)₃) (CCDC-2062351): C₆₂H₅₅Ag₅F₉N₁₇O₉S₃, $M = 1988.76$, monoclinic, space group C2/c (No. 15), $a = 38.1353(5)$ Å, $b = 21.9159(4)$ Å, $c = 25.6721(3)$ Å, $\beta = 129.9700(10)^\circ$, $V = 16443.4(5)$ Å³, $Z = 8$, $T = 173.00(10)$ K, $D_c = 1.607$ g cm⁻³. The structure, refined on F^2 , converged for 15513 unique reflections ($R_{\text{int}} = 0.0268$) and 14298 observed reflections with $I > 2\sigma(I)$ to give $R_1 = 0.0532$ and $wR_2 = 0.1656$ and a goodness-of-fit = 1.061. The SQUEEZE procedure of PLATON was used in the processing of **PhPyAg₅**. The checkCIF report of **PhPyAg₅** has a B alert of “Hirshfeld Test Diff for S2-O84”. This can be ascribed to the disorders of triflate anions in the structure of **PhPyAg₅**.

Crystal data for MePyAg₁₃ ([Ag₁₃(C₆NH₅)₆H₆](CF₃SO₃)₆) (CCDC-1995296): C₄₂H₃₆Ag₁₃F₁₈N₆O₁₈S₆, $M = 2849.44$, triclinic, space group P-1 (No. 2), $a = 14.0332(7)$ Å, $b = 15.3545(7)$ Å, $c = 22.4180(9)$ Å, $\alpha = 82.805(4)^\circ$, $\beta = 84.350(3)^\circ$, $\gamma = 88.156(4)^\circ$, $V = 4768.2(4)$ Å³, $Z = 2$, $T = 293$ K, $D_c = 1.985$ g cm⁻³. The structure, refined on F^2 , converged for 18877 unique reflections ($R_{\text{int}} = 0.099$) and 10657 observed reflections with $I > 2\sigma(I)$ to give $R_1 = 0.1681$ and $wR_2 = 0.4685$ and a goodness-of-fit = 1.195. The SQUEEZE procedure of PLATON was used in the processing of **MePyAg₁₃**. There is an A alert of “Check Calcd Positive Resid. Density on Ag” in the checkCIF report, which can be ascribed to the Fourier truncation error induced by the metal atom. The B alert of “High wR₂ Value (i.e. > 0.25)” is attributed to a little low signal to noise ratio of the crystal data and the other two B alerts can be ascribed to the disorders of triflate anions in the structure of **MePyAg₁₃**.

Crystal data for *n*-PrPyAg₁₃ ([Ag₁₃(C₈NH₉)₆H₆](CF₃SO₃)₆) (CCDC-2062348): C₅₄H₆₀Ag₁₃F₁₈N₆O₁₈S₆, $M = 3017.75$, triclinic, space group P-1 (No. 2), $a = 14.2592(3)$ Å, $b = 17.1159(6)$ Å, $c = 21.9955(6)$ Å, $\alpha = 96.598(2)^\circ$, $\beta = 93.982(2)^\circ$, $\gamma = 92.905(2)^\circ$, $V = 5310.4(3)$ Å³, $Z = 2$, $T = 100$ K, $D_c = 1.887$ g cm⁻³. The structure, refined on F^2 , converged for 21079 unique reflections ($R_{\text{int}} = 0.0750$) and 13952 observed reflections with $I > 2\sigma(I)$ to give $R_1 = 0.0893$ and $wR_2 = 0.2813$ and a goodness-of-fit = 1.035. The checkCIF report of ***n*-PrPyAg₁₃** has an A alert of “Check Calcd Positive Resid. Density on Ag6”, which can be ascribed to the Fourier truncation error induced by

the metal atom. And the two B alerts of “High ‘MainMol’ Ueq as Compared to Neighbors of O01G” and “Low Bond Precision on C-C Bond” can be attributed to the disorders of triflate anions in the structure of *n*-PrPyAg₁₃.

Crystal data for ^{Ph}PyAg₁₃ ([Ag₁₃(C₁₁NH₇)₆H₆](CF₃SO₃)₆) (CCDC-2062349): C₇₂H₄₈Ag₁₃F₁₈N₆O₁₈S₆, *M* = 3221.83, orthorhombic, space group Fddd (No. 70), *a* = 16.1557(9) Å, *b* = 30.2077(17) Å, *c* = 58.888(4) Å, α = 90°, β = 90°, γ = 90°, *V* = 28739(3) Å³, *Z* = 8, *T* = 296.15 K, *Dc* = 1.627 g cm⁻³. The structure, refined on *F*², converged for 8802 unique reflections (*R*_{int} = 0.0882) and 5651 observed reflections with *I* > 2σ(*I*) to give *R*₁ = 0.1340 and *wR*₂ = 0.4077 and a goodness-of-fit = 1.080. The SQUEEZE procedure of PLATON was used in the processing of ^{Ph}PyAg₁₃. In the checkCIF report of ^{Ph}PyAg₁₃, there is a B alert of “High wR₂ Value (i.e. > 0.25)” that can be ascribed to a few smeared reflections in the crystal data, presumably due to the disordered benzene within the crystal causing the bad packing. And the other four B alerts can be ascribed to the disorders of triflate anions and benzene rings in the structure of ^{Ph}PyAg₁₃.

Crystal data for protonated 2,2'-dimethyl-4,4'-bipyridine [C₁₂N₂H₁₄](SO₃CF₃)₂ (CCDC-1995303): C₁₄H₁₄F₆N₂O₆S₂, *M* = 434.38, triclinic, space group P-1 (No. 2), *a* = 14.2592(3) Å, *b* = 17.1159(6) Å, *c* = 21.9955(6) Å, α = 96.598(2)°, β = 93.982(2)°, γ = 92.905(2)°, *V* = 5310.4(3) Å³, *Z* = 2, *T* = 99.99(10) K, *Dc* = 1.682 g cm⁻³. The structure, refined on *F*², converged for 1908 unique reflections (*R*_{int} = 0.0456) and 1659 observed reflections with *I* > 2σ(*I*) to give *R*₁ = 0.0565 and *wR*₂ = 0.1583 and a goodness-of-fit = 1.037. The checkCIF report has a B alert of “diffrn_measured_fraction_theta_full value Low 0.955”, which may be ascribed to a few missing data points at theta-max angle.

Crystal data for protonated 2,2'-dipropyl-4,4'-bipyridine [C₁₆N₂H₂₂](SO₃CF₃)₂ (CCDC-2060712): C₁₈H₂₂F₆N₂O₆S₂, *M* = 540.51, triclinic, space group P-1 (No. 2), *a* = 9.0344(3) Å, *b* = 12.9270(4) Å, *c* = 15.4280(5) Å, α = 85.714(2)°, β = 87.099(3)°, γ = 87.475(3)°, *V* = 1792.99(10) Å³, *Z* = 3, *T* = 173 K, *Dc* = 1.5016 g cm⁻³. The structure, refined on *F*², converged for 6033 unique reflections (*R*_{int} = 0.0271) and 4852 observed reflections with *I* > 2σ(*I*) to give *R*₁ = 0.0632 and *wR*₂ = 0.1791 and a goodness-of-fit = 1.057.

Crystal data for (Py[8]-2H⁺-Ag⁺)(OTf)₃ [Ag(Py[8]-2H)](SO₃CF₃)₃ (CCDC-2175048): C₅₁H₅₀AgF₉N₁₆O₉S₃, *M* = 1406.12, monoclinic, space group *P2*₁/*c* (No. 14), *a* = 13.6223(2) Å, *b* = 29.4112(4) Å, *c* = 17.5734(3) Å, β = 111.122(2)°, *V* = 6567.72(19) Å³, *Z* = 4, *T* = 173 K, *Dc* = 1.422 g cm⁻³. The structure, refined on *F*², converged for 12564 unique reflections (*R*_{int} = 0.0220) and 10845 observed reflections with *I* > 2σ(*I*) to give *R*₁ = 0.0567 and *wR*₂ = 0.1602 and a goodness-of-fit = 1.034.

3. Supporting Figures

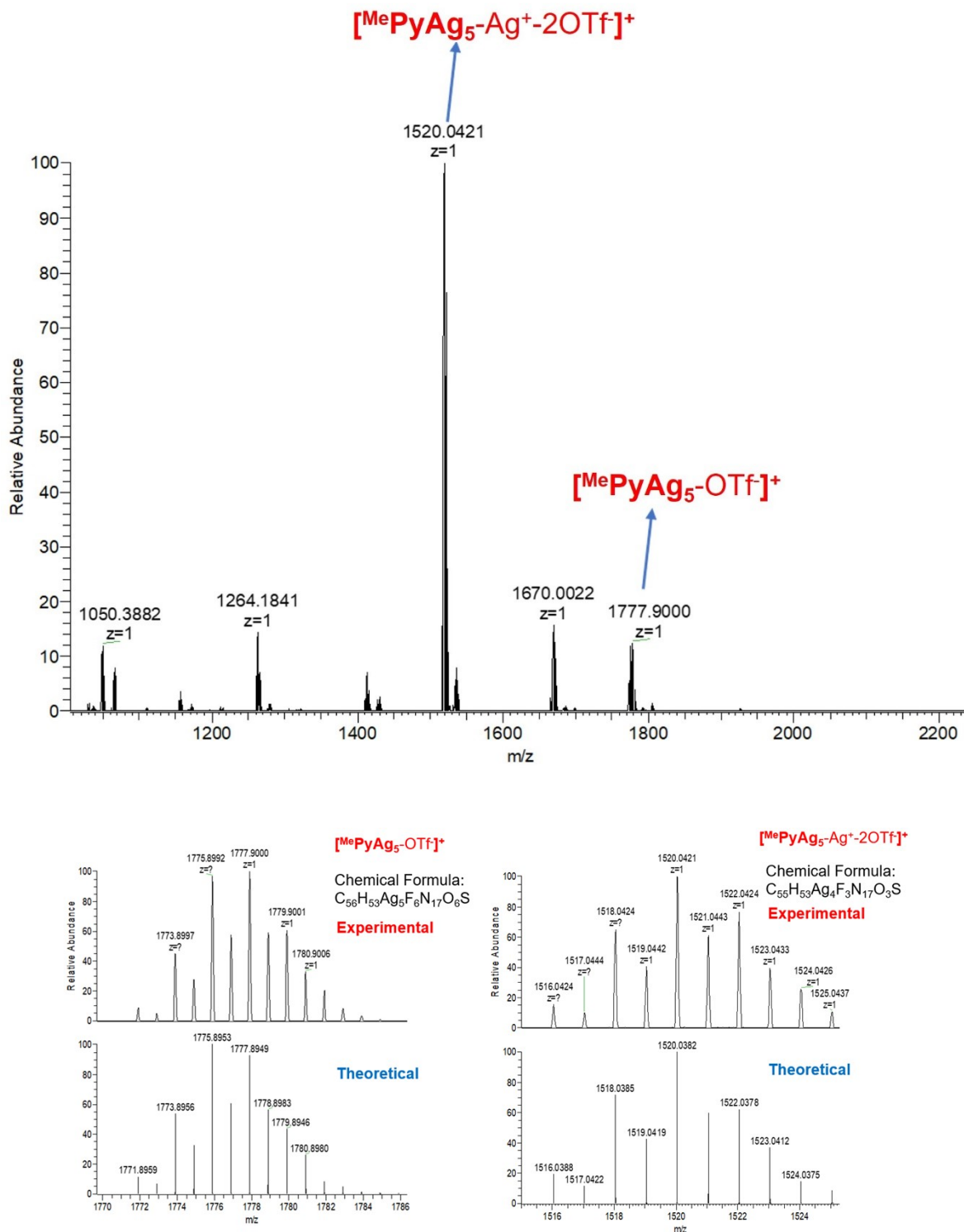


Figure S1. High resolution ESI-MS spectra of complex ^{Me}PyAg₅ in methanol. Calcd. for C₅₆H₅₃Ag₅F₆N₁₇O₆S 1777.8949 ([^{Me}PyAg₅ - OTf]⁺), found 1777.9000 ([^{Me}PyAg₅ - OTf]⁺); Calcd. for C₅₅H₅₃Ag₄F₃N₁₇O₃S 1520.0382 ([^{Me}PyAg₅ - Ag⁺ - 2OTf]⁺), found 1520.0421 ([^{Me}PyAg₅ - Ag⁺ - 2OTf]⁺).

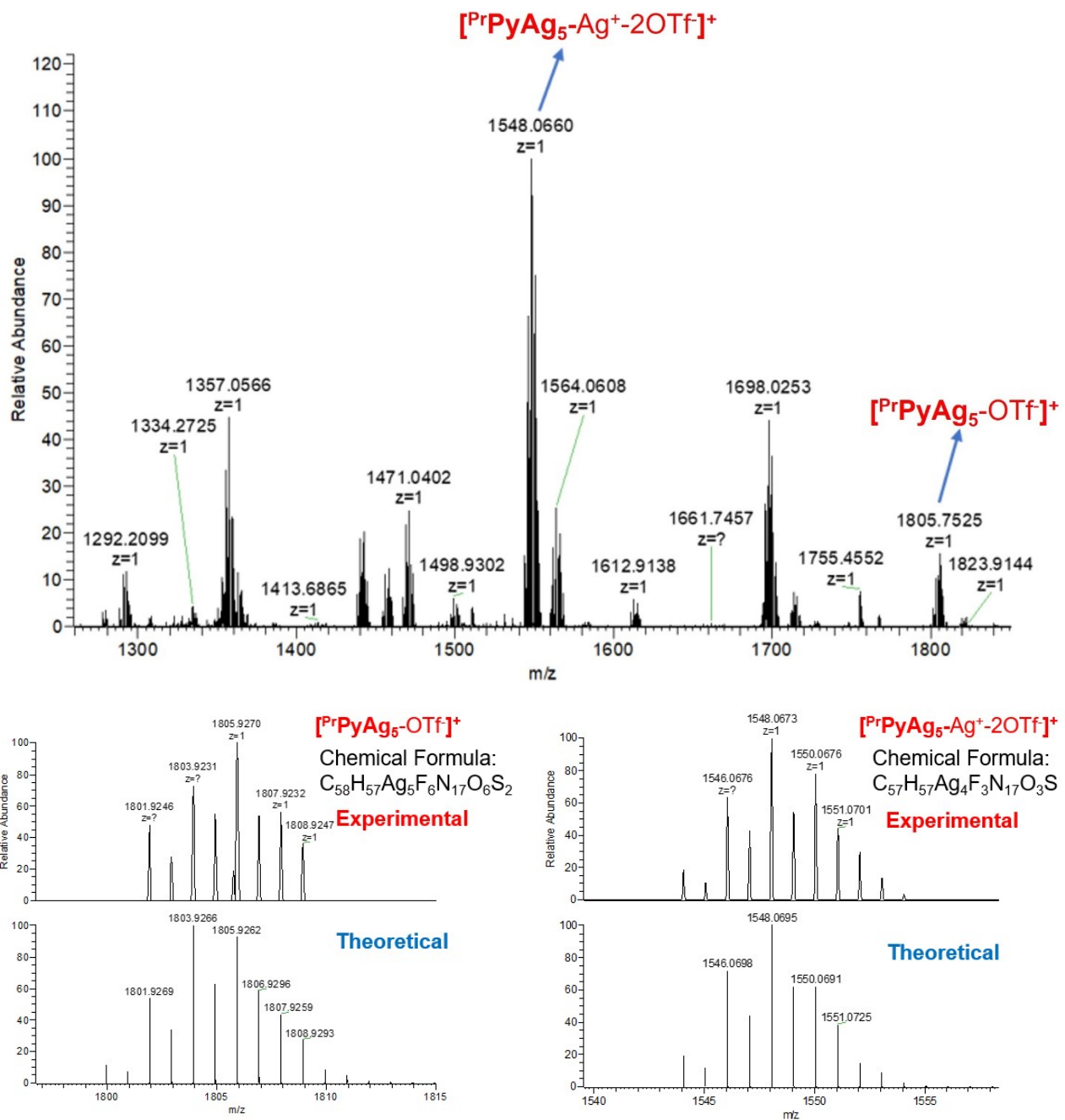


Figure S2. High resolution ESI-MS spectra of complex ⁿ-PrPyAg₅ in methanol. Calcd. for C₅₈H₅₇Ag₅F₆N₁₇O₆S₂ 1805.9262 ([ⁿ-PrPyAg₅-OTf]⁺), found 1805.9270 ([ⁿ-PrPyAg₅-OTf]⁺); Calcd. for C₅₇H₅₇Ag₄F₃N₁₇O₃S 1548.0695 ([ⁿ-PrPyAg₅-Ag⁺-2OTf]⁺), found 1548.0673 ([ⁿ-PrPyAg₅-Ag⁺-2OTf]⁺).

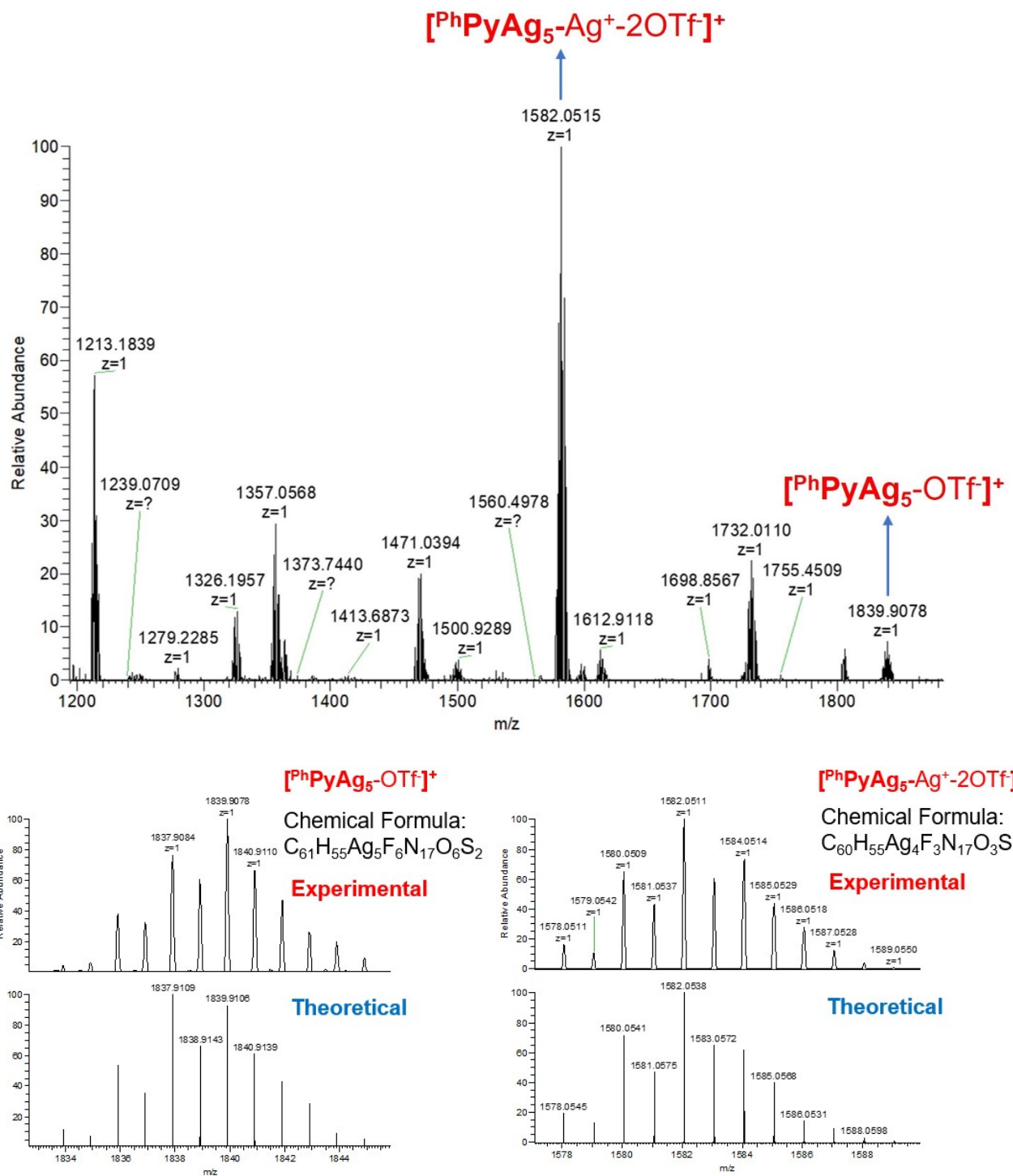


Figure S3. High resolution ESI-MS spectra of complex ^{Ph}PyAg₅ in methanol. Calcd. for C₆₁H₅₅Ag₅F₆N₁₇O₆S 1839.9106 ([^{Ph}PyAg₅ - OTf]⁺), found 1839.9078 ([^{Ph}PyAg₅ - OTf]⁺); Calcd. for C₆₀H₅₅Ag₄F₃N₁₇O₃S 1582.0538 ([^{Ph}PyAg₅ - Ag⁺ - 2OTf]⁺), found 1582.0511 ([^{Ph}PyAg₅ - Ag⁺ - 2OTf]⁺).

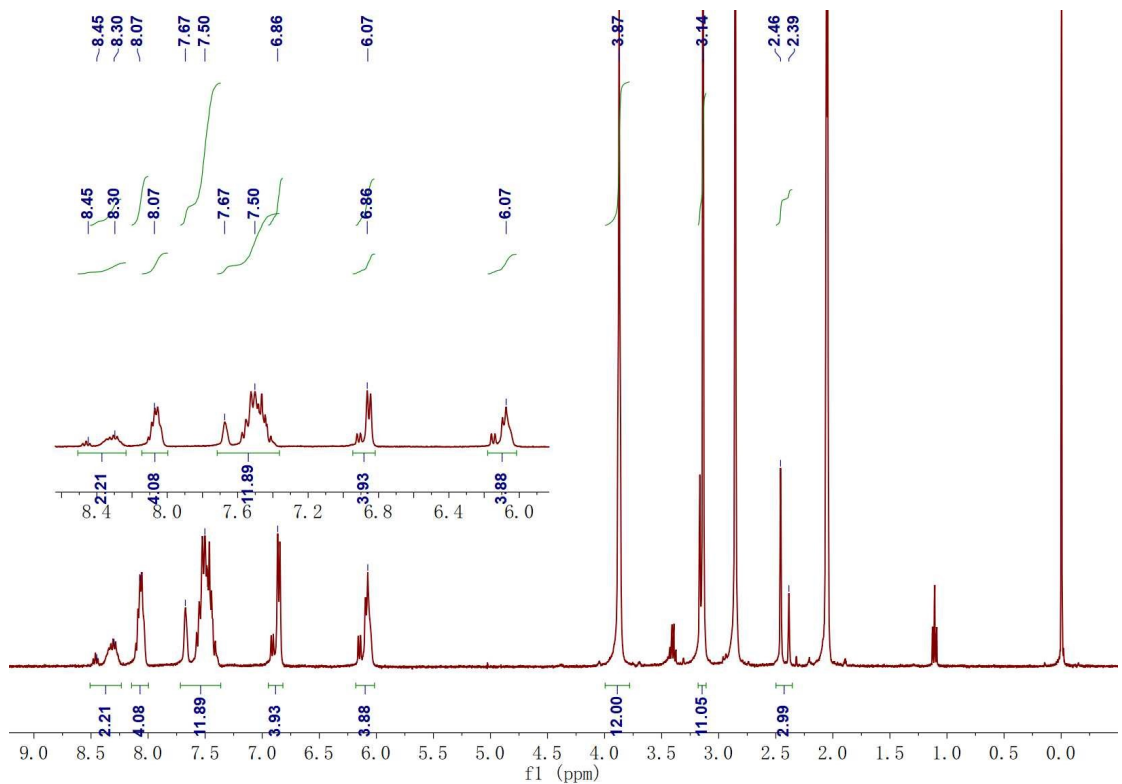


Figure S4. ^1H -NMR spectrum of complex MePyAg_5 (400 MHz, d_6 -acetone, 298 K).

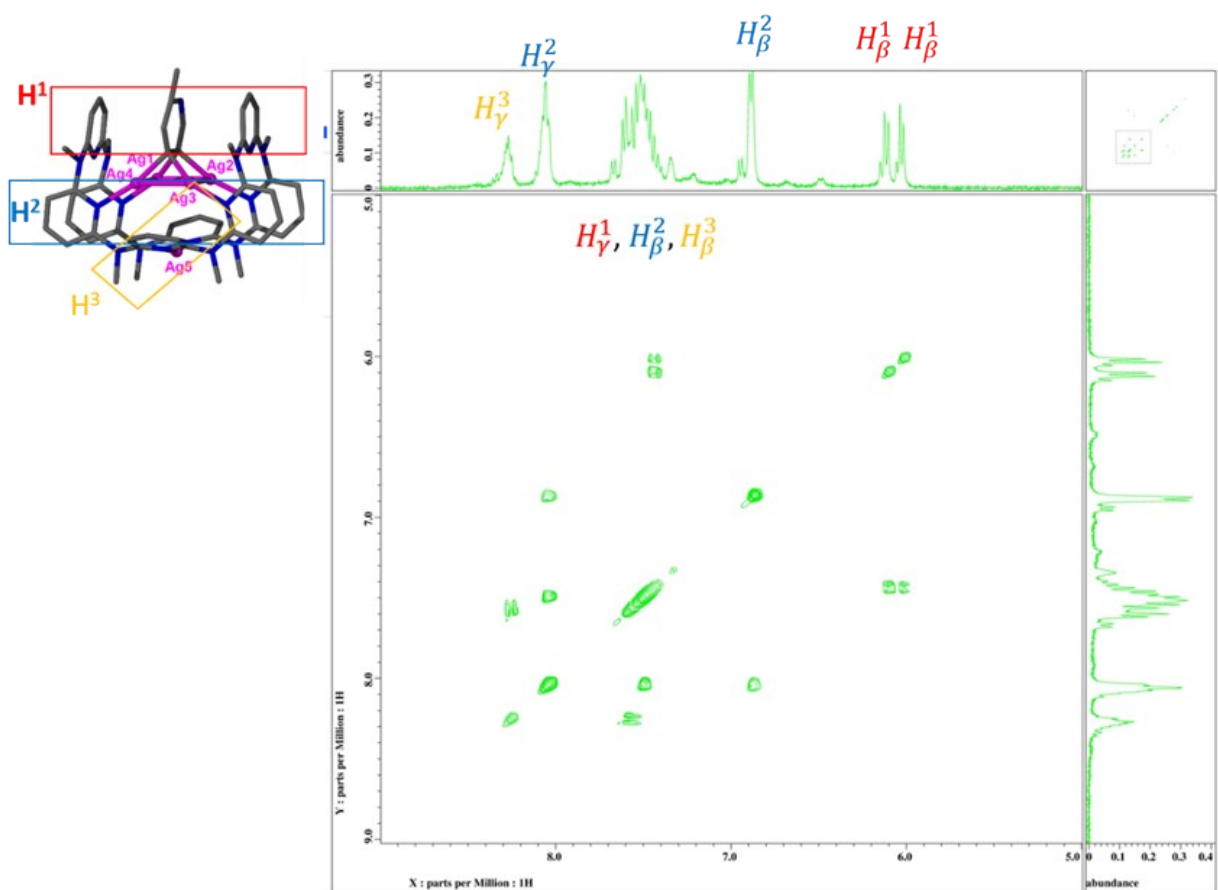


Figure S5. Partial ^1H -COSY spectrum of ${}^{\text{Me}}\text{PyAg}_5$ in d_6 -acetone at -60 °C.

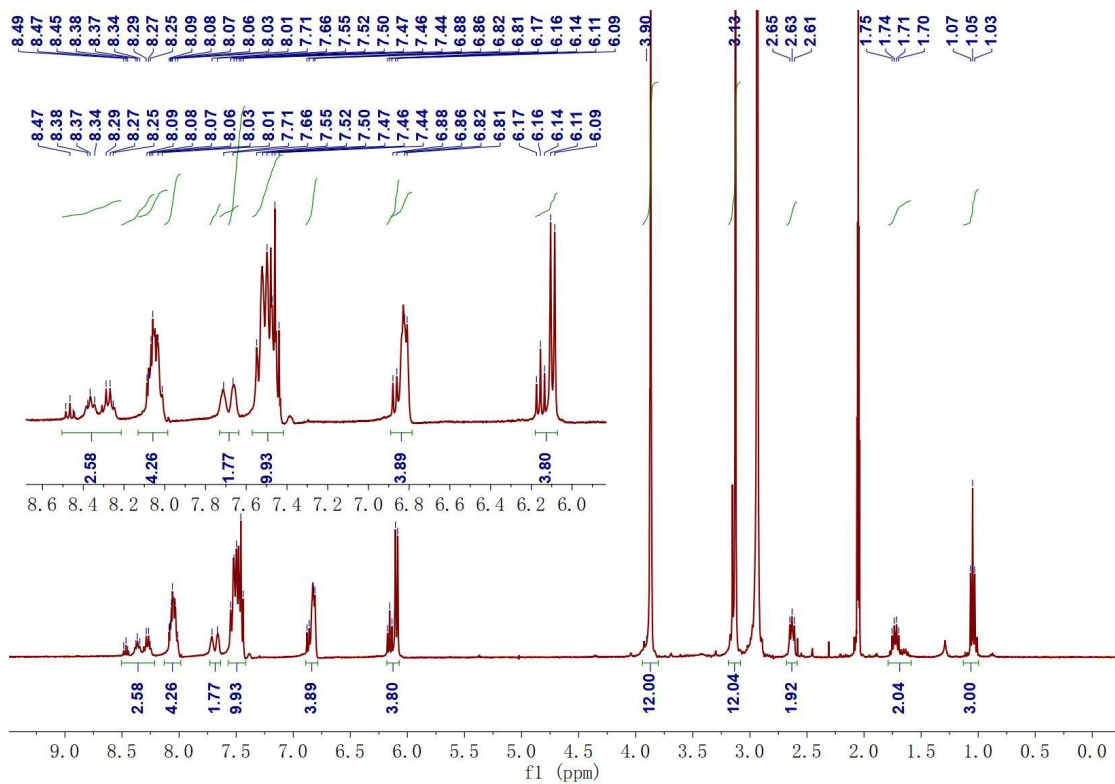


Figure S6. ^1H -NMR spectrum of complex $n\text{-PrPyAg}_5$ (400 MHz, d_6 -acetone, 298 K).

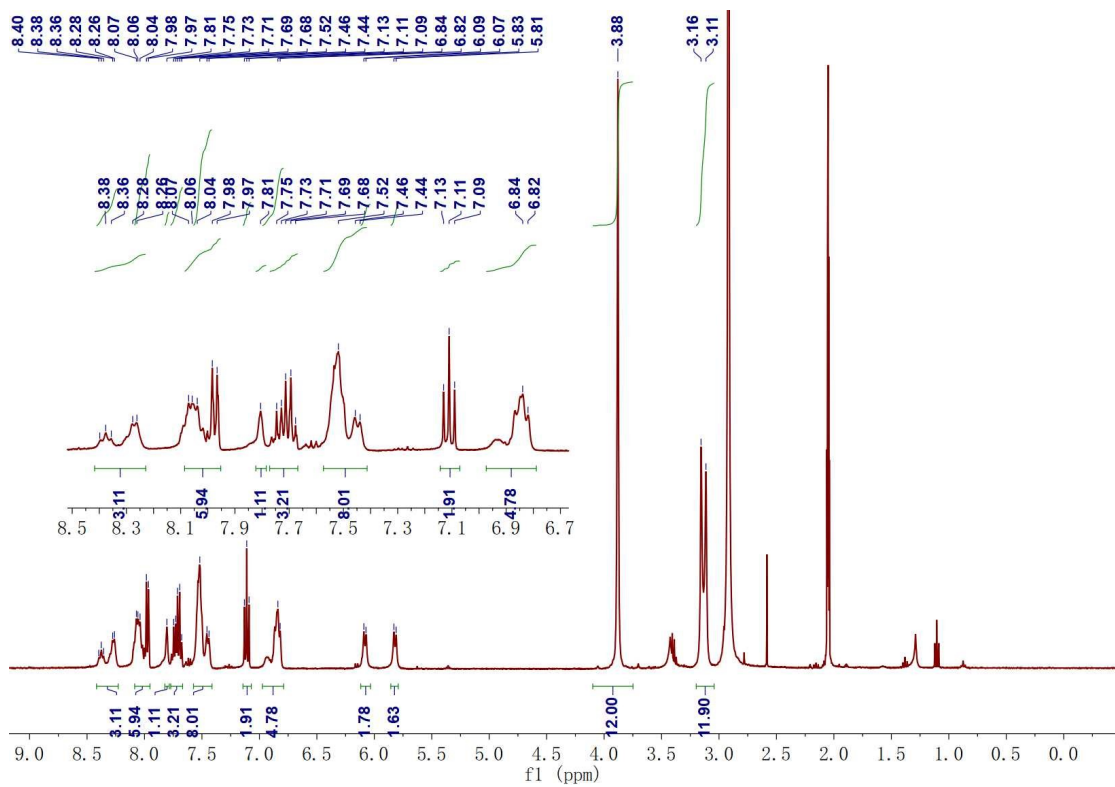


Figure S7. ^1H -NMR spectrum of complex ${}^{\text{Ph}}\text{PyAg}_5$ (400 MHz, d_6 -acetone, 298 K).

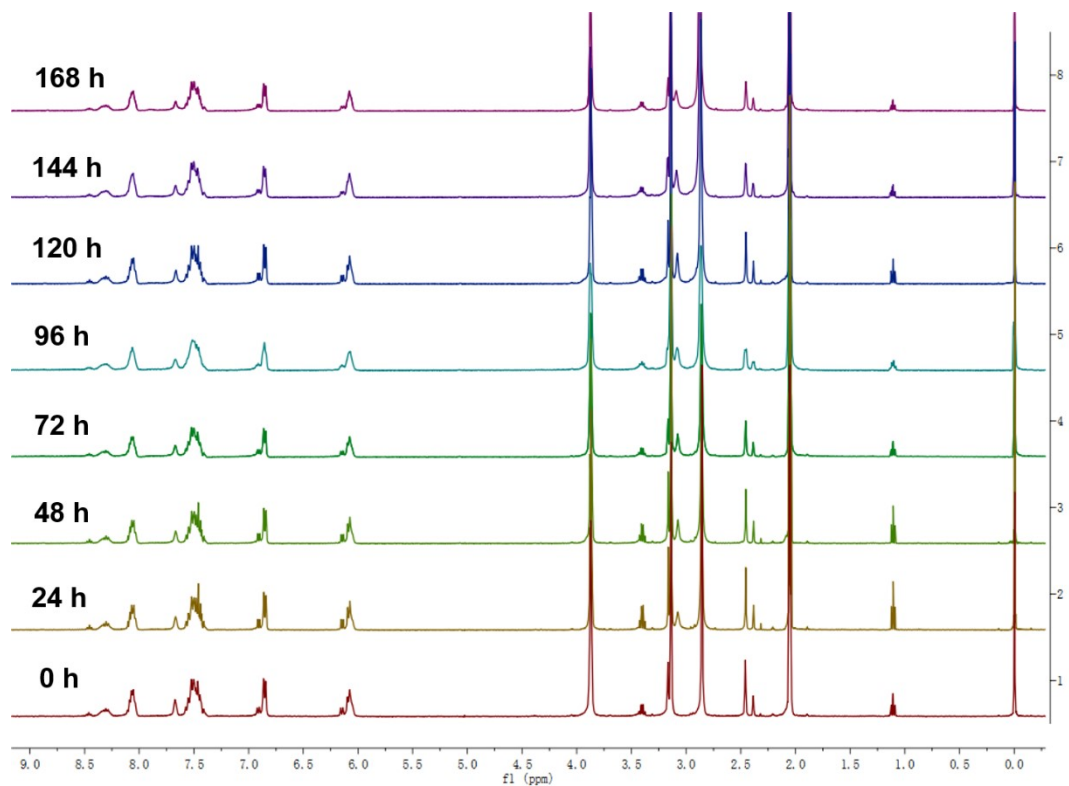


Figure S8. Time-dependent ^1H -NMR spectrum of complex MePyAg_5 (400 MHz, d_6 -acetone, 298 K).

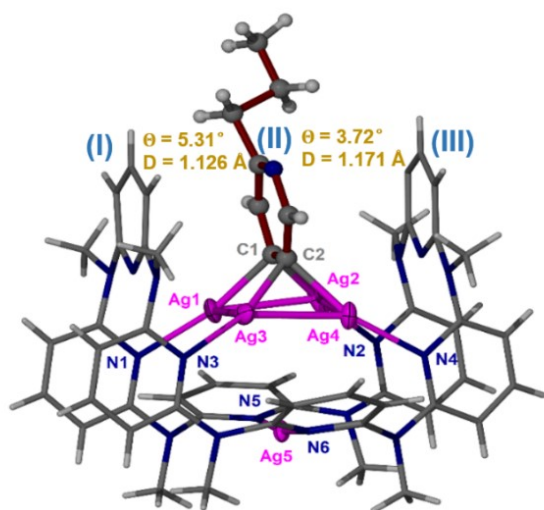


Figure S9. Crystal structure of $n\text{-PrPyAg}_5$. Peripheral CF_3SO_3^- anions are omitted for clarity. Color coding: Ag, purple (ellipsoids set at 40% probability); C, gray; H, white; N, blue. Selected bond lengths (\AA): Ag3-Ag4 2.725 (8); Ag1-Ag2 2.720 (9); Ag1-Ag3 3.362 (1); Ag2-Ag4 3.207 (9); C2-Ag3 2.191 (8); C2-Ag4 2.157 (9); C1-Ag1 2.193 (9); C1-Ag2 2.190 (1).

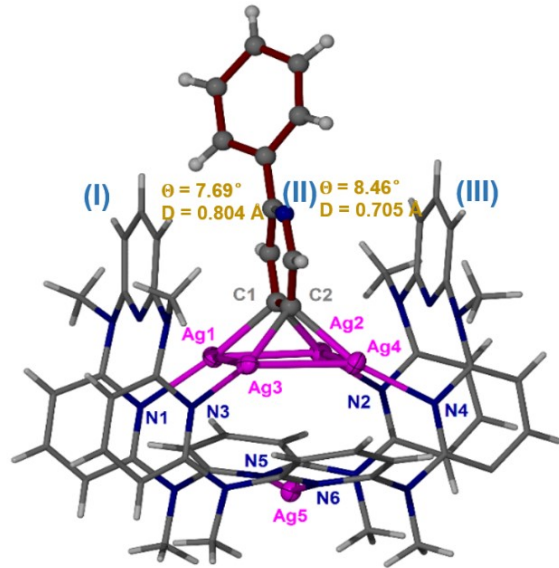


Figure S10. Crystal structure of $^{Ph}PyAg_5$. Peripheral $CF_3SO_3^-$ anions are omitted for clarity. Color coding: Ag, purple (ellipsoids set at 40% probability); C, gray; H, white; N, blue. Selected bond lengths (\AA): Ag3-Ag4 2.743(6); Ag1-Ag2 2.699(6); Ag1-Ag3 3.324(6); Ag2-Ag4 3.182(6); C2-Ag3 2.173(5); C2-Ag4 2.166(5); C1-Ag1 2.202(5); C1-Ag2 2.162(5).

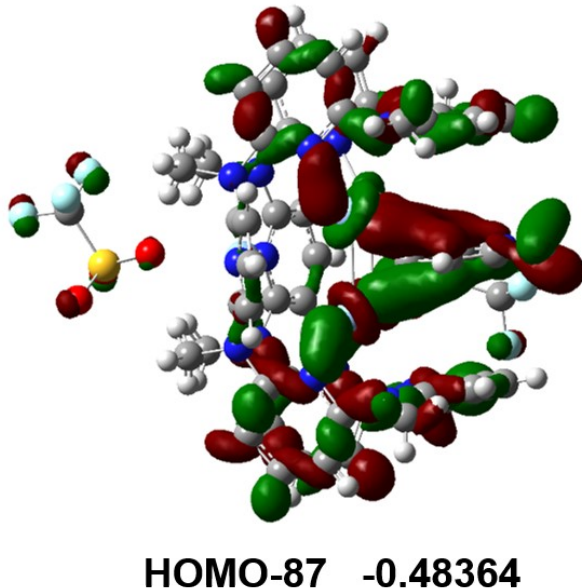


Figure S11. Molecular orbitals of $^{Me}PyAg_5$ manifesting the participation of p_{π} orbitals of pyridine ring in the bonding with silver atoms. The energy is given in atomic unit.

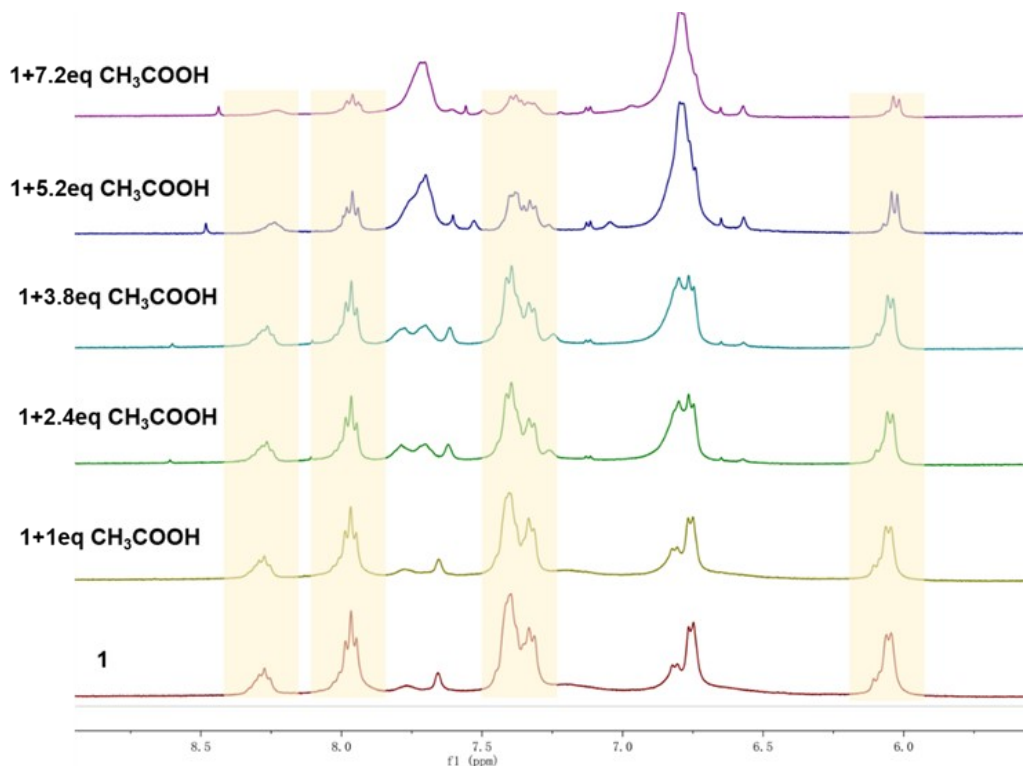


Figure S12. Partial ¹H NMR spectra (400 MHz, *d*₆-acetone) of ^{MePyAg₅} in the CH₃COOH titration experiment.

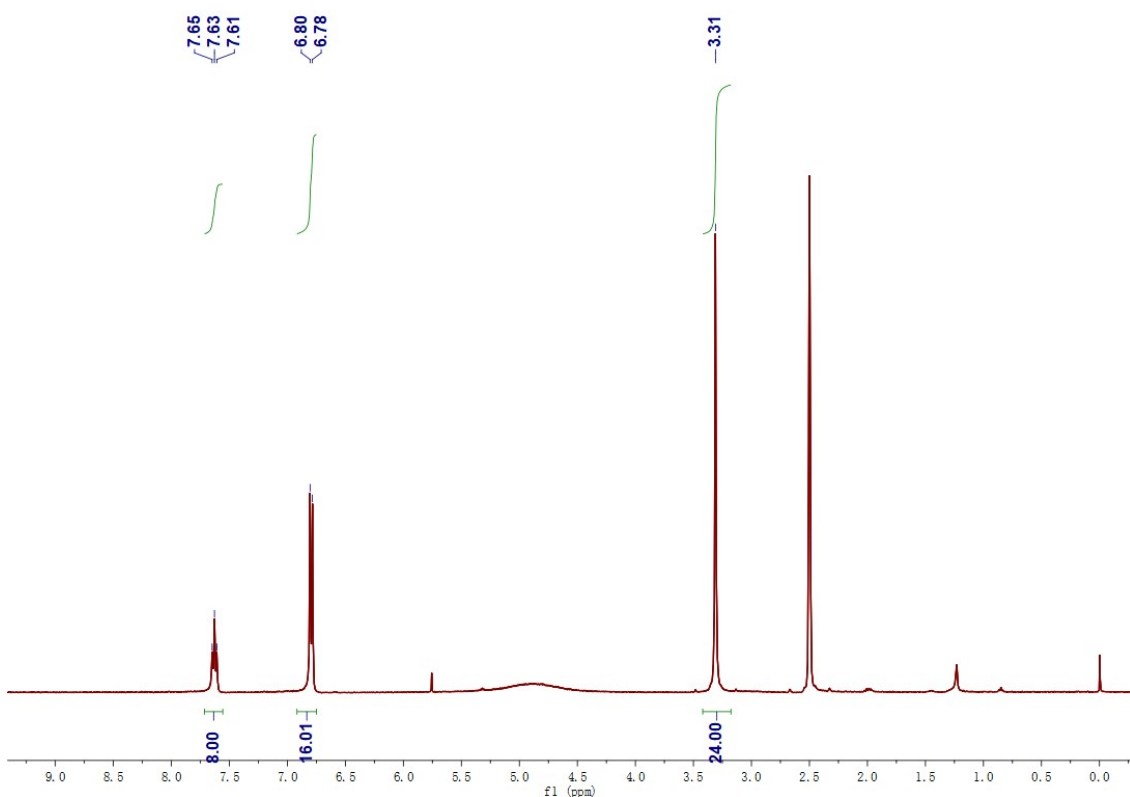


Figure S13. ¹H-NMR spectrum of white precipitate (^{Py[8]-2H⁺-Ag⁺}(OTf)₃) after adding HOTf into ^{MePyAg₅} (400 MHz, *d*₆-DMSO, 298 K).

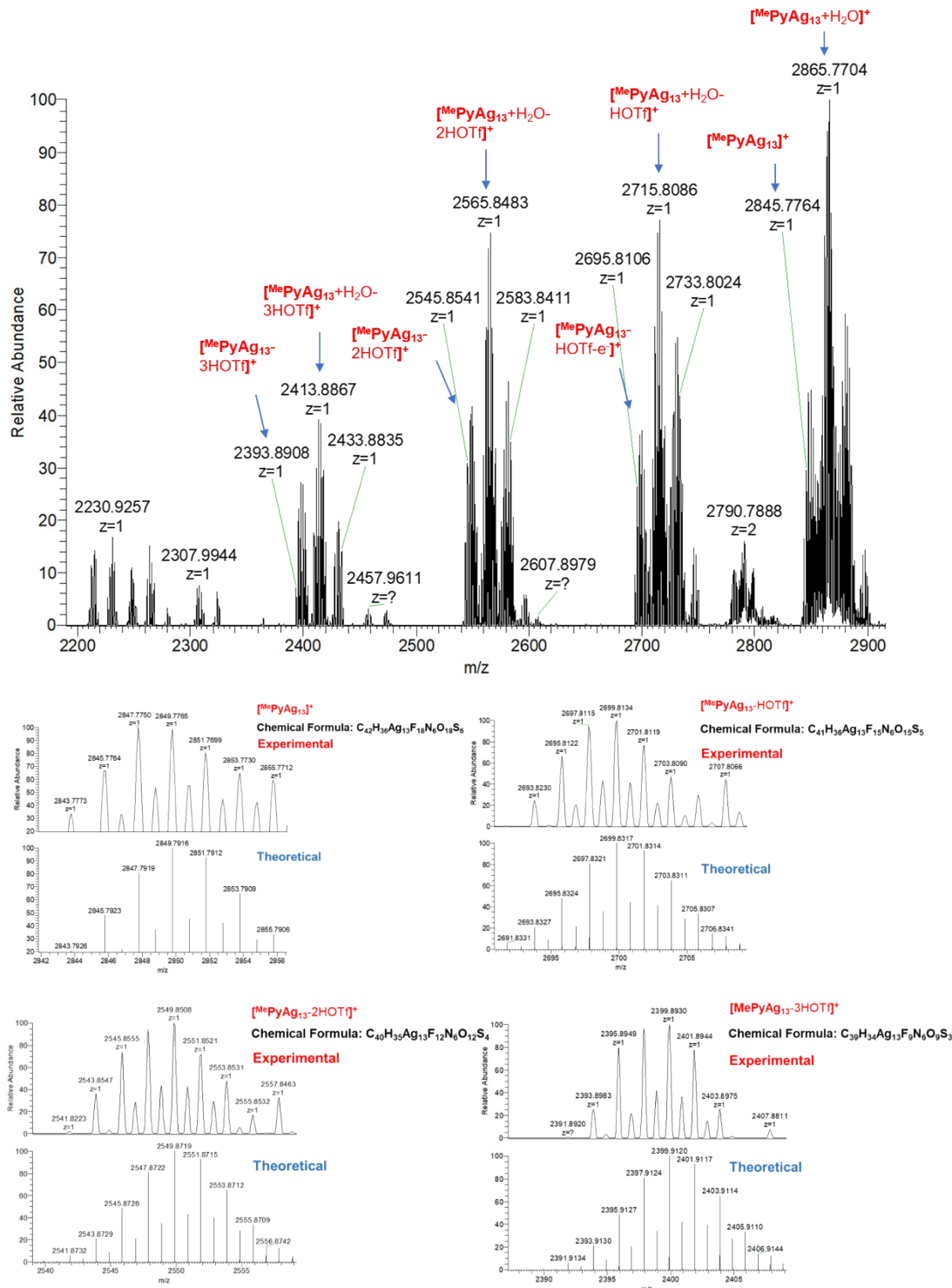


Figure S14. High resolution ESI-MS spectra of MePyAg_{13} in acetone. Calcd. for $\text{C}_{42}\text{H}_{36}\text{Ag}_{13}\text{F}_{18}\text{N}_6\text{O}_{18}\text{S}_6$ 2847.7719 ($[\text{MePyAg}_{13}]^+$), found 2847.7750 ($[\text{MePyAg}_{13}]^+$); Calcd. for $\text{C}_{42}\text{H}_{38}\text{Ag}_{13}\text{F}_{18}\text{N}_6\text{O}_{19}\text{S}_6$ 2865.7865 ($[\text{MePyAg}_{13} \bullet \text{H}_2\text{O}]^+$), found 2865.7704 ($[\text{MePyAg}_{13} \bullet \text{H}_2\text{O}]^+$); Calcd. for $\text{C}_{41}\text{H}_{36}\text{Ag}_{13}\text{F}_{15}\text{N}_6\text{O}_{15}\text{S}_5$ 2699.8317 ($[\text{MePyAg}_{13} - \text{HOTf}]^+$), found 2699.8314 ($[\text{MePyAg}_{13} - \text{HOTf}]^+$); Calcd. for $\text{C}_{40}\text{H}_{35}\text{Ag}_{13}\text{F}_{12}\text{N}_6\text{O}_{12}\text{S}_4$ 2549.8719 ($[\text{MePyAg}_{13} - 2\text{HOTf}]^+$), found 2549.8508 ($[\text{MePyAg}_{13} - 2\text{HOTf}]^+$); Calcd. for $\text{C}_{39}\text{H}_{34}\text{Ag}_{13}\text{F}_9\text{N}_6\text{O}_9\text{S}_3$ 2399.9120 ($[\text{MePyAg}_{13} - 3\text{HOTf}]^+$), found 2399.8930 ($[\text{MePyAg}_{13} - 3\text{HOTf}]^+$).

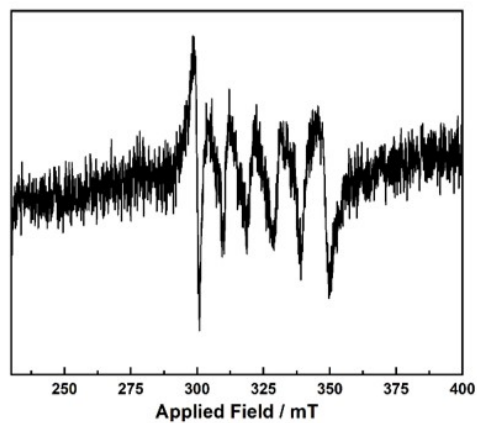


Figure S15. EPR spectra of $^{Me}PyAg_{13}$ at 153 K (EtOH:MeOH = 4:1).

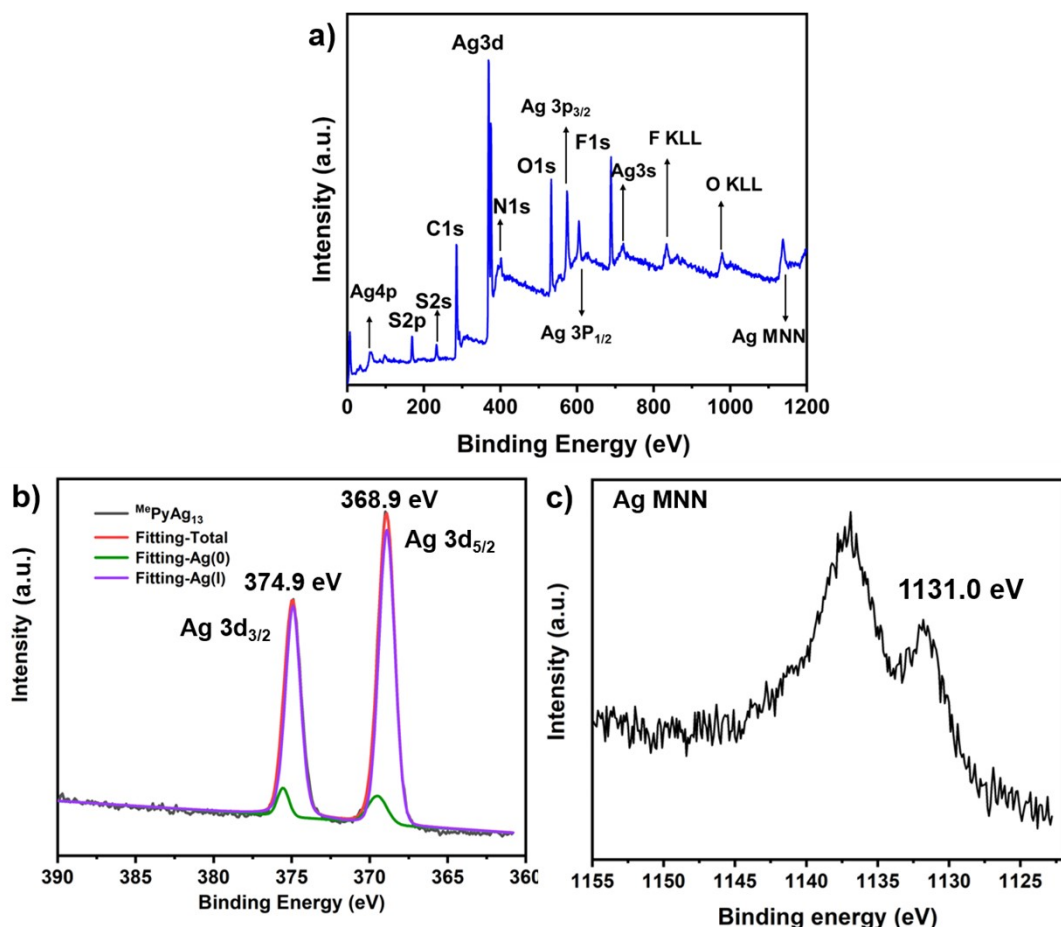


Figure S16. X-ray photoelectron spectra of $^{Me}PyAg_{13}$: survey spectrum (a), high-resolution spectra of Ag 3d (b) and Ag MNN 3d (c).

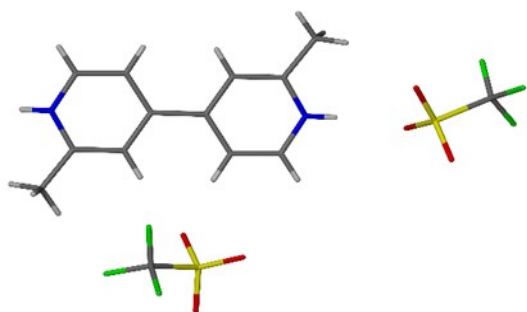


Figure S17. Crystal structure of the coupling product protonated 2,2'-dimethyl-4,4'-bipyridine. Color coding: C, gray; H, white; N, blue; S, yellow; O, red; F, brilliant blue.

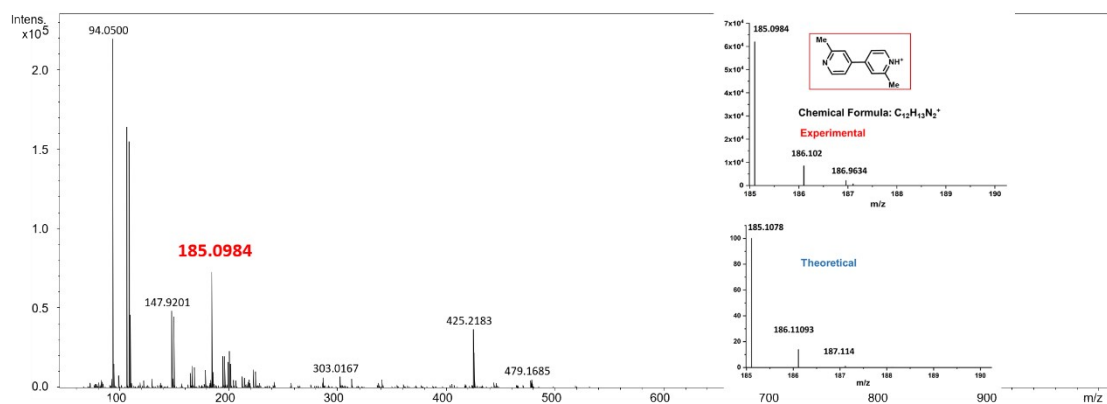


Figure S18. High resolution ESI-MS spectra of acidifying acetone solution of ${}^{\text{Me}}\text{PyAg}_5$.

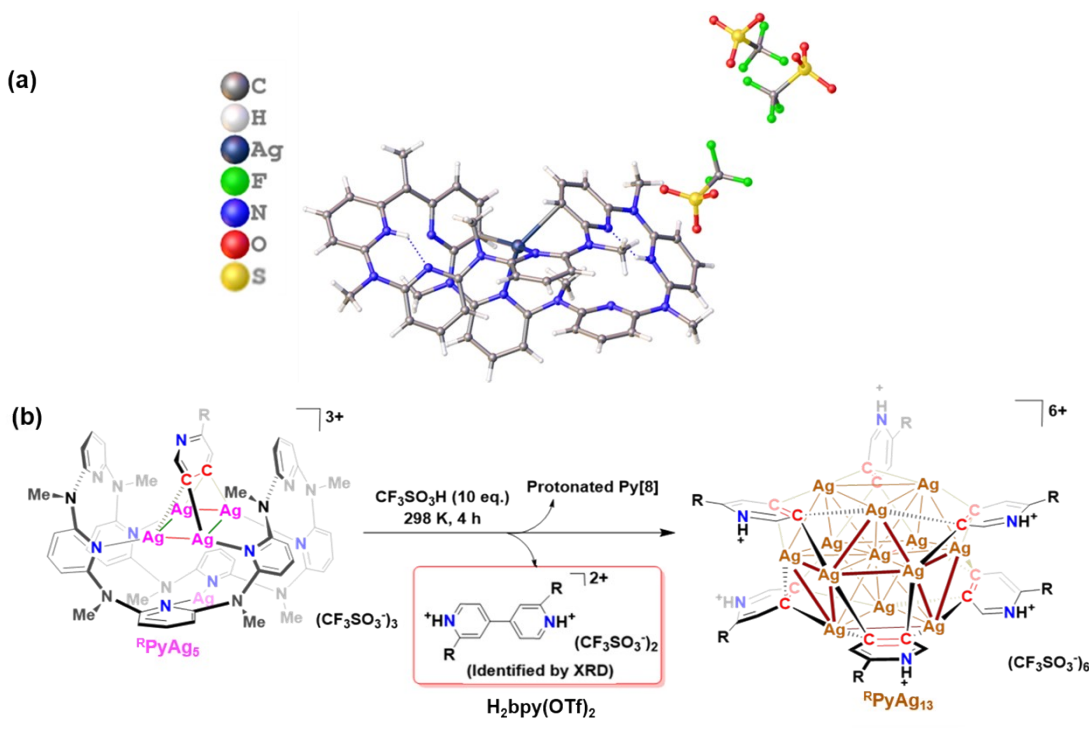


Figure S19. (a) The crystal structure of (**Py[8]**-2H⁺-Ag⁺)(OTf)₃ from the acidification of **RPyAg₅**; (b) Synthetic procedures for aryl vicinal dicarbanion bonded Ag₁₃ nanoclusters and the corresponding reaction equation of **MePyAg₅** and CF₃SO₃H as an example.

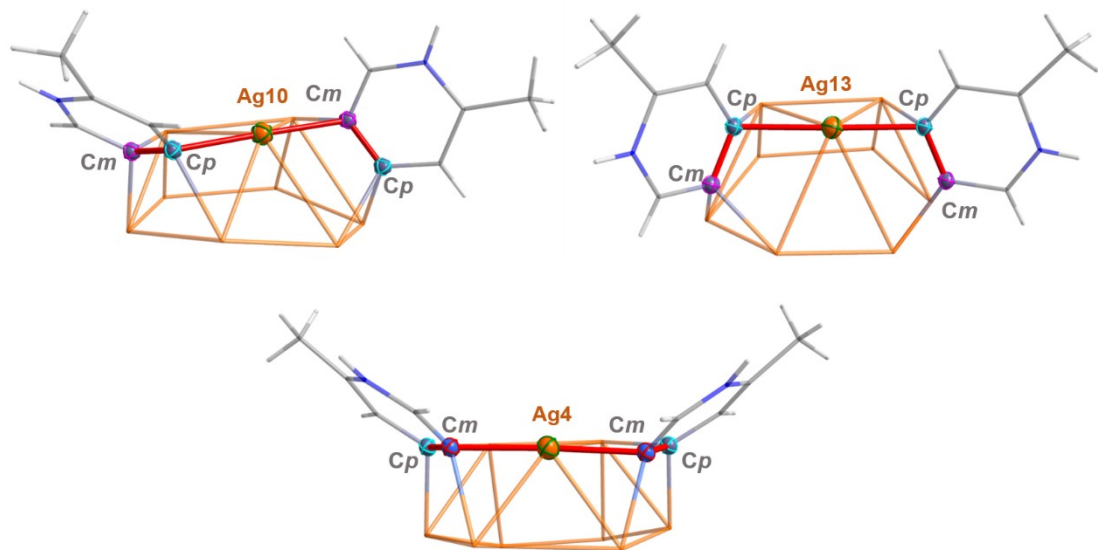


Figure S20. Three combinations of C_{para}-Ag-C_{para}, C_{para}-Ag-C_{meta} and C_{meta}-Ag-C_{meta} in **MePyAg₁₃**.

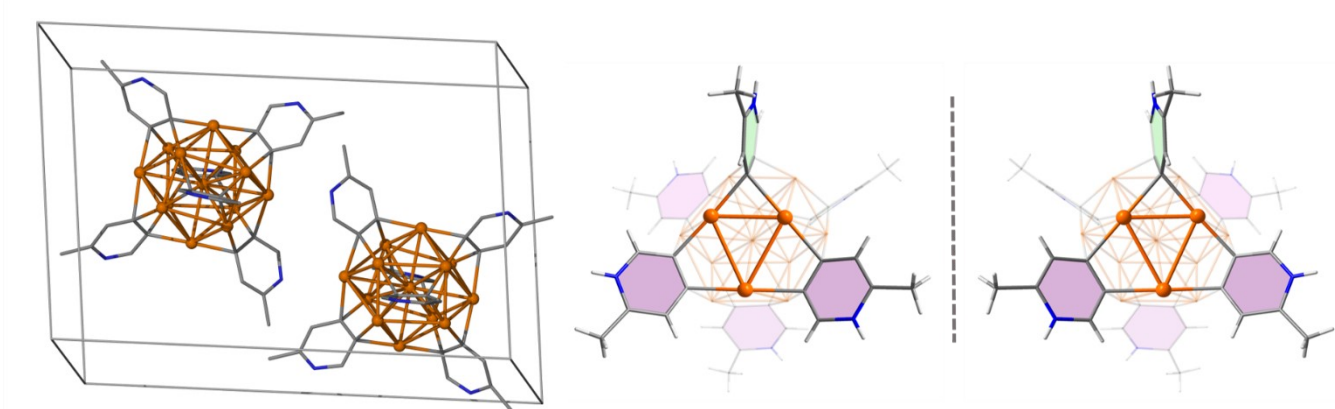


Figure S21. Two enantiomers co-exist in the crystal structure of **MePyAg₁₃**.

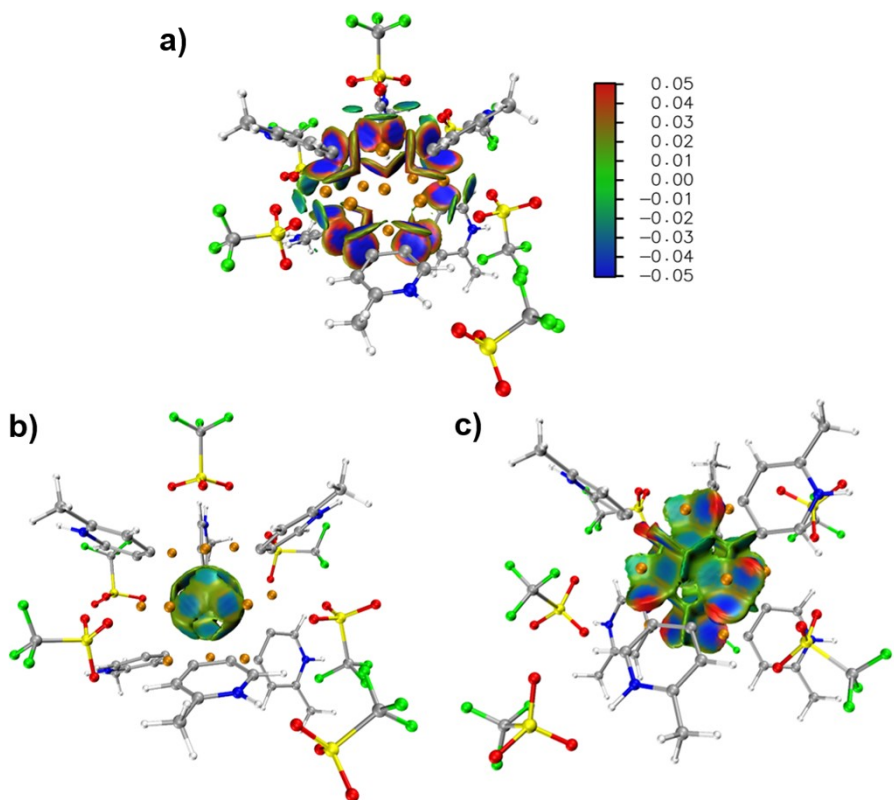


Figure S22. $\text{Sign}(\lambda_2)\rho$ colored IGMH map. a): $\delta g^{\text{inter}} = 0.015$ a.u. isosurfaces of MePyAg_{13} formed by six 2-methylpyridyl diides and Ag_{13} core; b): $\delta g^{\text{inter}} = 0.015$ a.u. isosurfaces of Ag_{13} core formed by central $\text{Ag}(0)$ atom and twelve surface silver ions; c): $\delta g^{\text{intra}} = 0.015$ a.u. isosurfaces of Ag_{13} core. Color scale is from -0.05 to 0.05 a.u. Red color (large and positive $\text{Sign}(\lambda_2)\rho$ value) denotes strong steric effect; blue color (large and negative $\text{Sign}(\lambda_2)\rho$ value) denotes attractive interaction.

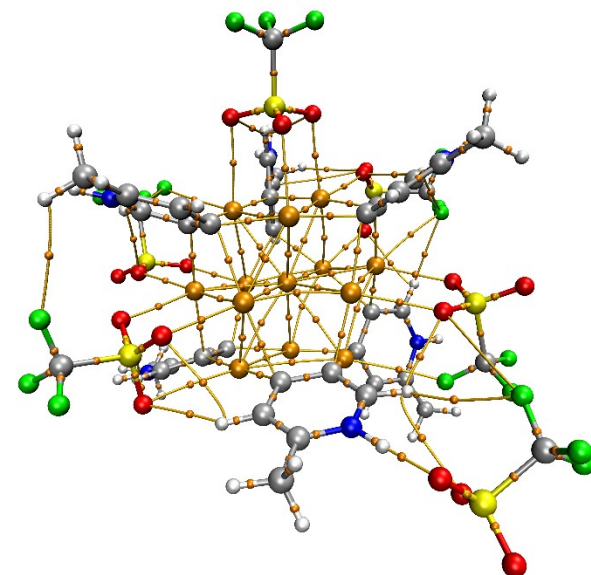


Figure S23. The BCPs of MePyAg_{13} in AIM analysis.

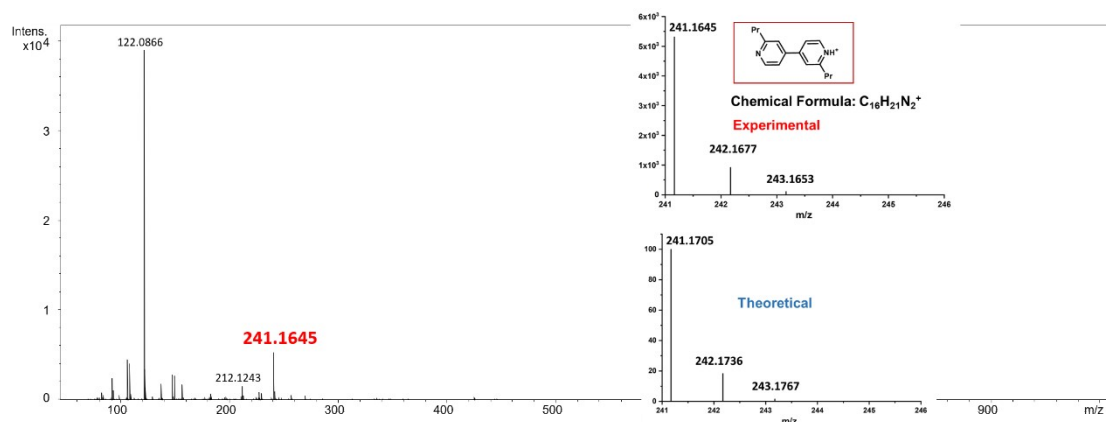


Figure S24. High resolution ESI-MS spectra of acidifying acetone solution of *n*-PrPyAg₅.

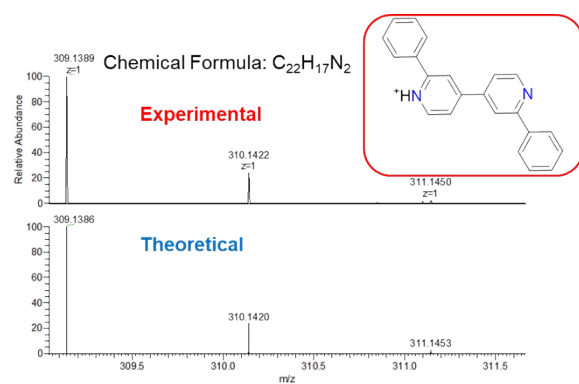


Figure S25. High resolution ESI-MS spectra of the coupling product 2,2'-diphenyl-4,4'-bipyridine.

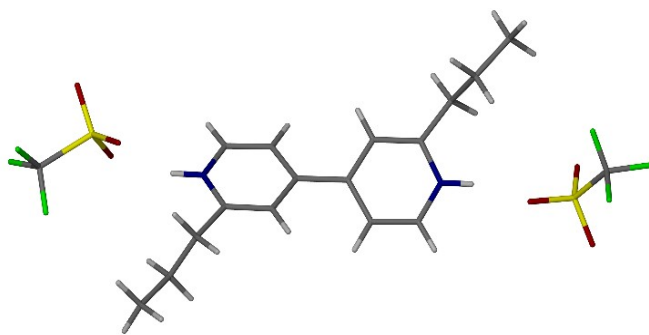


Figure S26. Crystal structure of the coupling product protonated 2,2'-dipropyl-4,4'-bipyridine. Color coding: C, gray; H, white; N, blue; S, yellow; O, red; F, brilliant blue.

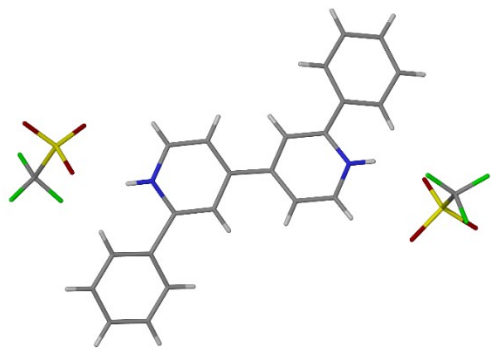


Figure S27. Crystal structure of the coupling product protonated 2,2'-diphenyl-4,4'-bipyridine. Color coding: C, gray; H, white; N, blue; S, yellow; O, red; F, brilliant blue. The completeness of the crystal data is not enough (80%) due to the quality of the crystal, but the single crystal structure can be precisely solved as shown above.

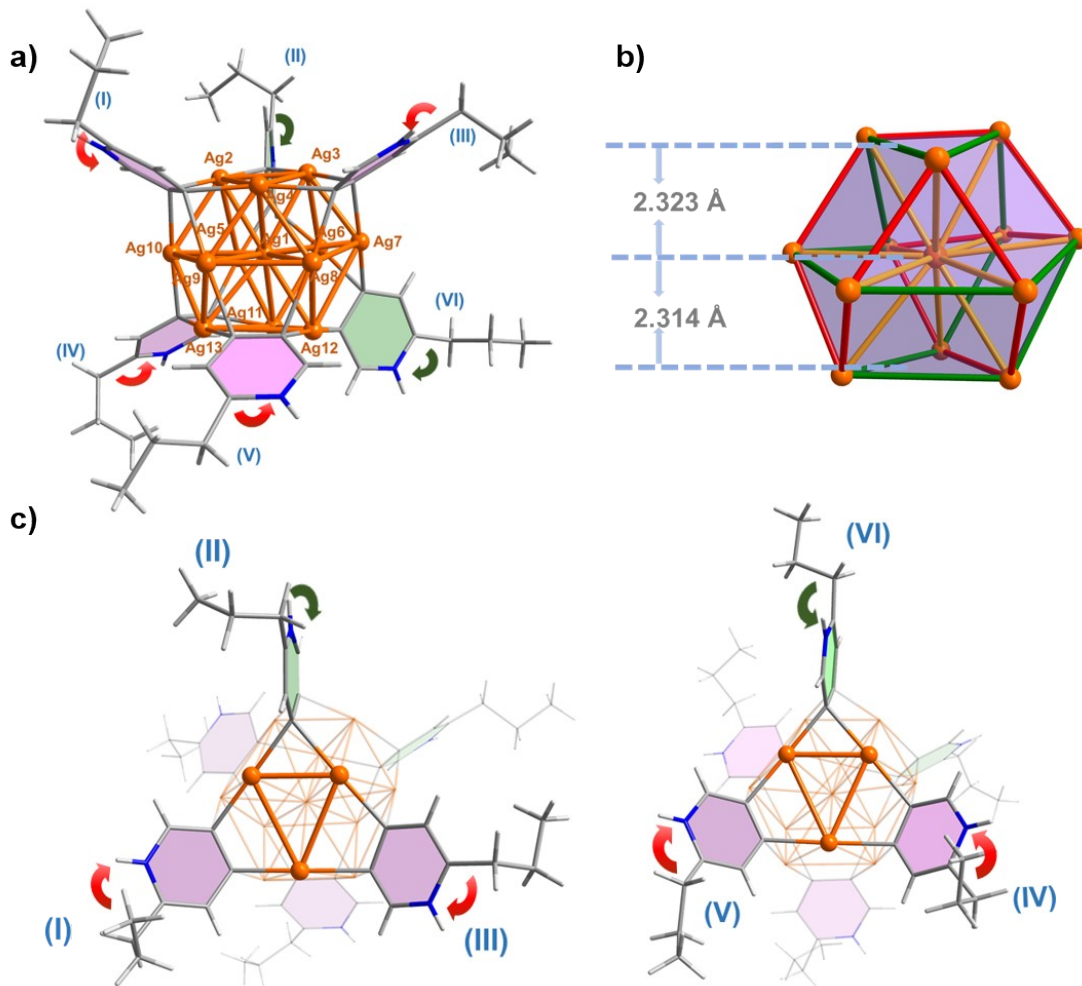


Figure S28. (a) Crystal structure of $n\text{-PrPyAg}_{13}$ containing equatorial (pink) and axial (light green) 2-propylpyridyl diide ligands. Peripheral CF_3SO_3^- anions are omitted for clarity; (b) The Ag_{13} kernel in $n\text{-PrPyAg}_{13}$. Color coding: Ag, brown; C, gray; H, white; N, blue. (c) Arrangement of the oriented 2-propylpyridine rings attached on the Ag_{13} kernel at the upper and nether sides in $n\text{-PrPyAg}_{13}$ (left: vertical view; right: upward view). Selected bond lengths (\AA) of $n\text{-PrPyAg}_{13}$ highlighted in yellow: Ag1-Ag2 2.877(1); Ag1-Ag3 2.927(1); Ag1-Ag4 2.980(1); Ag1-Ag5 2.977(1); Ag1-Ag6 3.160(1); Ag1-Ag7 2.983(1); Ag1-Ag8 2.962(1); Ag1-Ag9 3.014(1); Ag1-Ag10 2.914(1); Ag1-Ag11 2.980(1); Ag1-Ag12 2.866(2); Ag1-Ag13 3.013(1); red: Ag2-Ag3 2.762(1); Ag2-Ag10 2.828(1); Ag4-Ag9 2.730(1); Ag4-Ag8 2.747(2); Ag3-Ag7 2.738(2); Ag5-Ag6 2.717(1); Ag5-Ag11 2.740(2); Ag10-Ag13 2.730(1).

2.711(2); Ag9-Ag13 2.727(1); Ag8-Ag12 2.782(1); Ag6-Ag7 2.706(1); Ag11-Ag12 2.782(1); green: Ag2-Ag4 3.314(1); Ag3-Ag4 3.256(1); Ag10-Ag9 3.126(1); Ag8-Ag7 3.248(1); Ag2-Ag5 3.275(1); Ag3-Ag6 3.086(1); Ag5-Ag10 3.175(1); Ag11-Ag13 3.226(2); Ag8-Ag9 3.053(1); Ag12-Ag13 3.327(2); Ag7-Ag12 3.222(1); Ag6-Ag11 3.113(1).

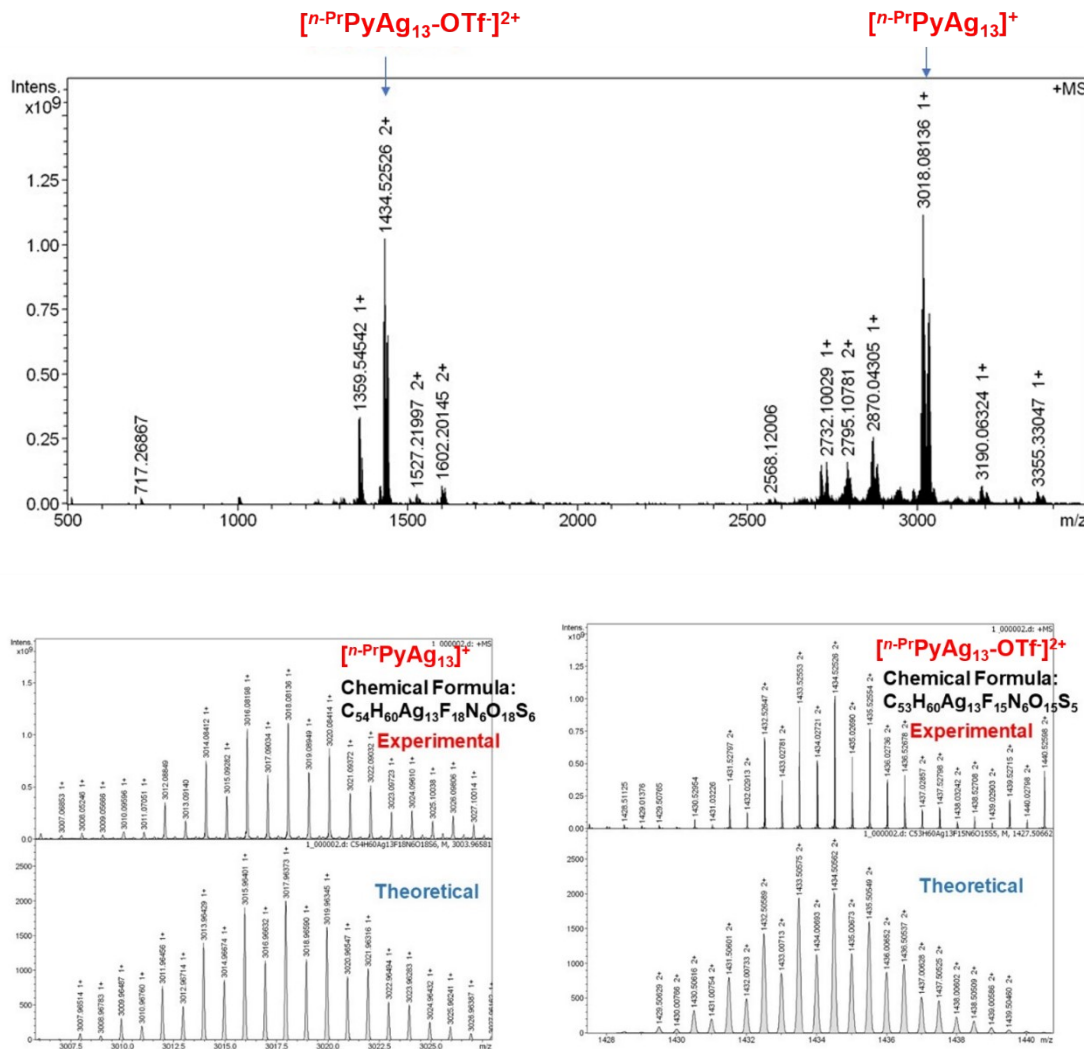


Figure S29. High resolution ESI-MS spectra of complex *n*-PrPyAg₁₃ in acetone. Calcd. for C₅₄H₆₀Ag₁₃F₁₈N₆O₁₈S₆ 3017.9637 ([*n*-PrPyAg₁₃]⁺), found 3018.0814 ([*n*-PrPyAg₁₃]⁺); Calcd. for C₅₃H₆₀Ag₁₃F₁₅N₆O₁₅S₅ 1434.5058 ([*n*-PrPyAg₁₃-OTf]²⁺), found 1434.5253 ([*n*-PrPyAg₁₃-OTf]²⁺).

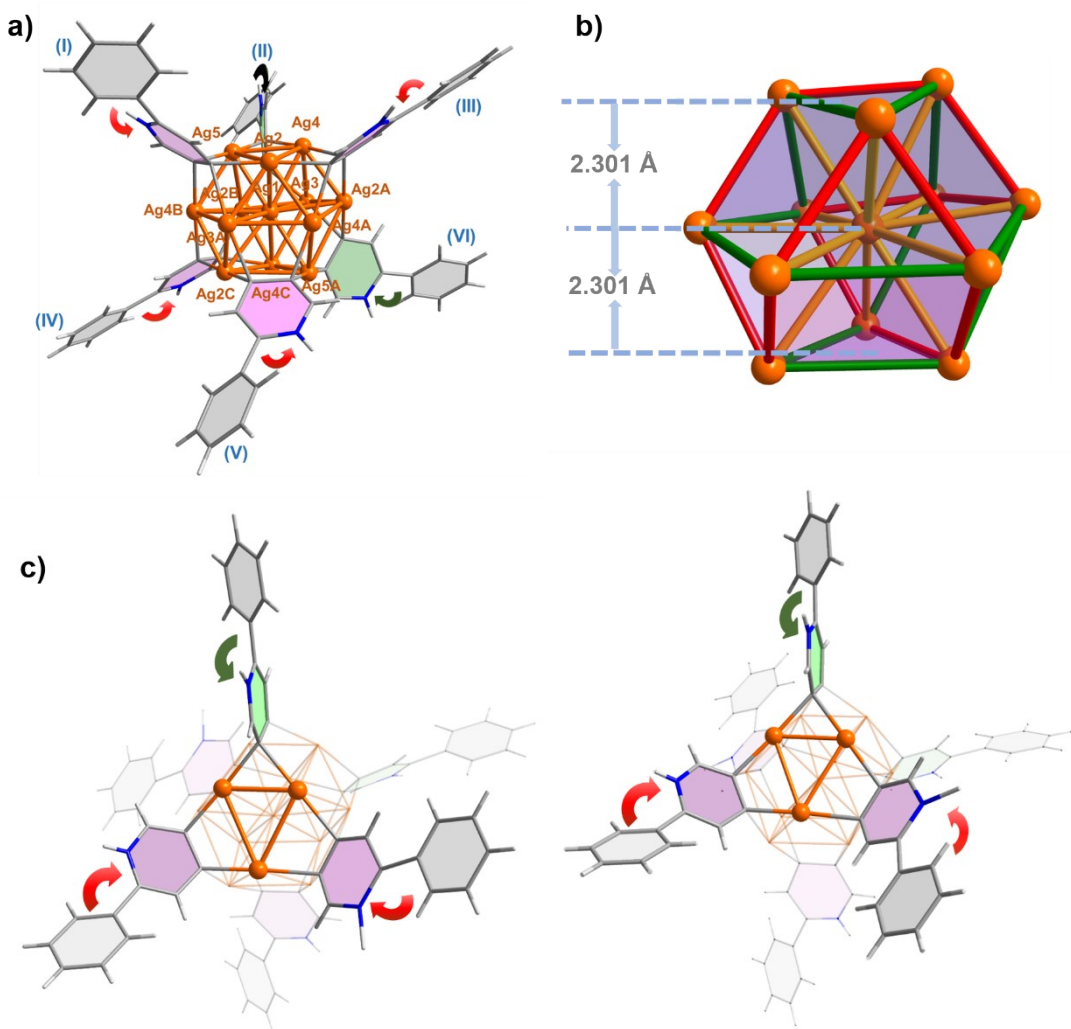


Figure S30. (a) Crystal structure of ${}^{\text{Ph}}\text{PyAg}_{13}$ containing equatorial (pink) and axial (light green) 2-phenylpyridyl diide ligands. Peripheral CF_3SO_3^- anions are omitted for clarity; (b) The Ag_{13} kernel in ${}^{\text{Ph}}\text{PyAg}_{13}$. Color coding: Ag, brown; C, gray; H, white; N, blue. (c) Arrangement of the orientated 2-phenylpyridine rings attached on the Ag_{13} kernel at the upper and nether sides in ${}^{\text{Ph}}\text{PyAg}_{13}$ (left: vertical view; right: upward view). Selected bond lengths (\AA) of ${}^{\text{Ph}}\text{PyAg}_{13}$ highlighted in yellow: Ag1-Ag2 2.968(1); Ag1-Ag3 3.150(1); Ag1-Ag4 2.941(1); Ag1-Ag5 2.828(1); red: Ag2-Ag2B 2.742(2); Ag5-Ag4B 2.799(2); Ag2-Ag4A 2.726(1); Ag3-Ag2B 2.742(2); green: Ag2-Ag5 3.217(2); Ag2-Ag4 3.220(2); Ag3A-Ag4B 3.110(1); Ag5A-Ag2C 3.217(2).

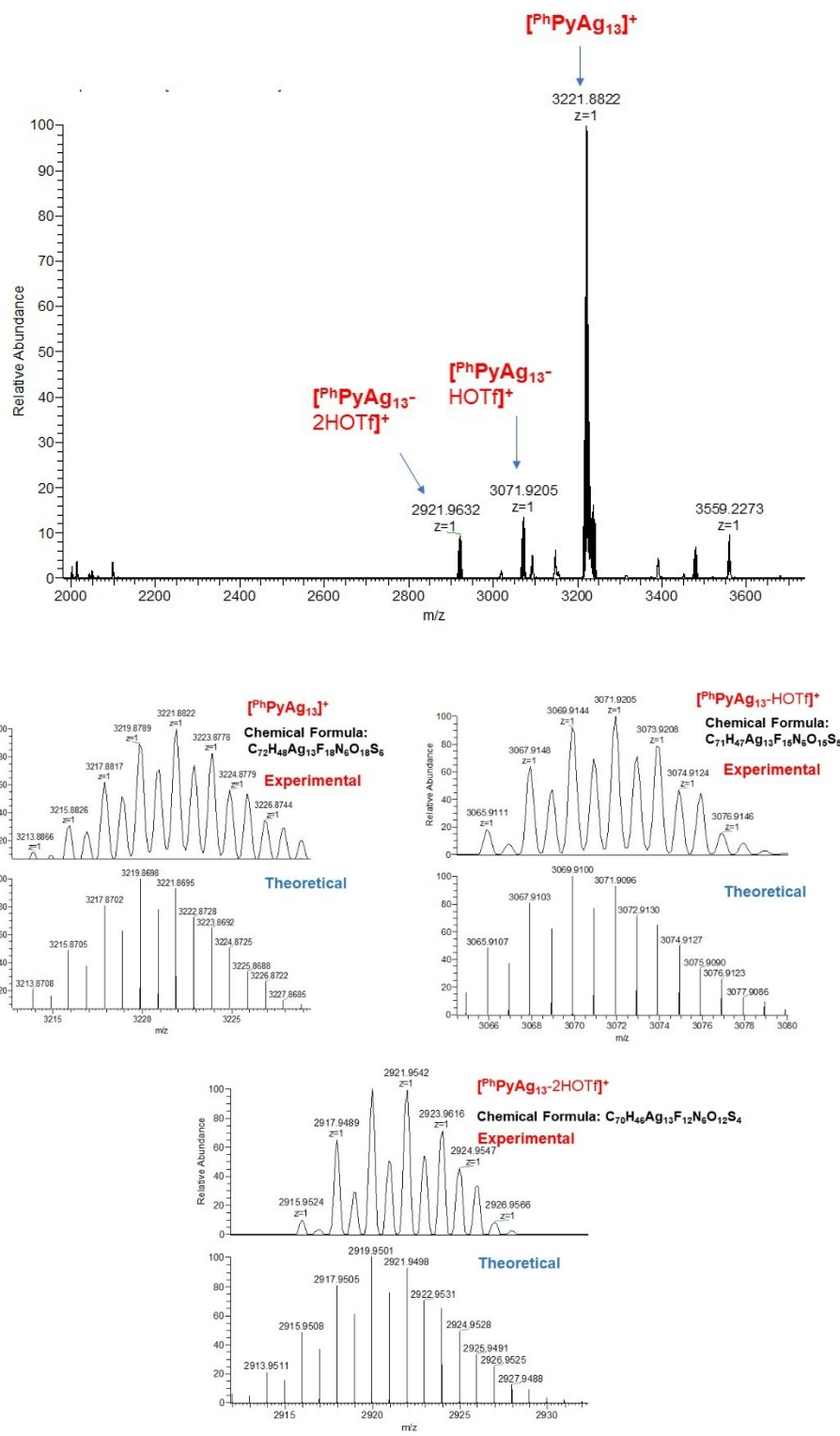


Figure S31. High resolution ESI-MS spectra of complex ^{Ph}PyAg₁₃ in acetone. Calcd. for $C_{72}H_{48}Ag_{13}F_{18}N_6O_{18}S_6$ 3221.8695 ($[^{Ph}PyAg_{13}]^+$), found 3221.8822 ($[^{Ph}PyAg_{13}]^+$); Calcd. for $C_{71}H_{47}Ag_{13}F_{15}N_6O_{15}S_5$ 3071.9096 ($[^{Ph}PyAg_{13}-HOTf]^+$), found 3071.9205 ($[^{Ph}PyAg_{13}-HOTf]^+$); Calcd. for $C_{70}H_{46}Ag_{13}F_{12}N_6O_{12}S_4$ 2921.9498 ($[^{Ph}PyAg_{13}-2HOTf]^+$), found 2921.9542 ($[^{Ph}PyAg_{13}-2HOTf]^+$).

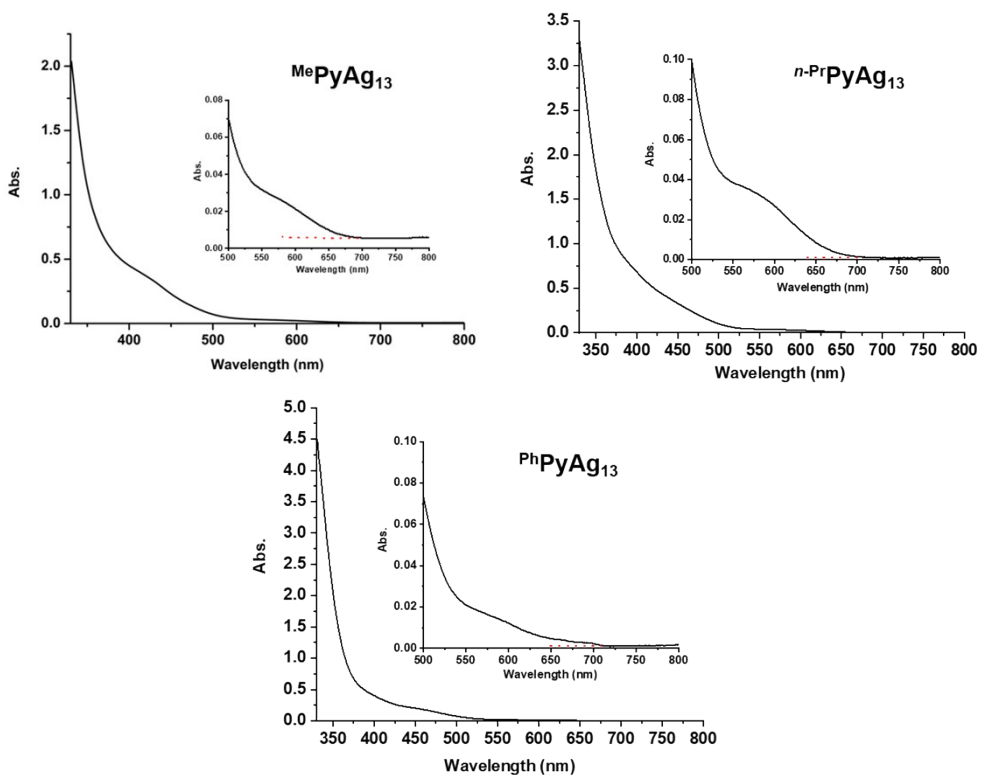


Figure S32. UV-vis spectra of $^{\text{Me}}\text{PyAg}_{13}$, $^{\text{n-Pr}}\text{PyAg}_{13}$ and $^{\text{Ph}}\text{PyAg}_{13}$ in acetone ($C = 2.5 \times 10^{-5}$ mol/L, 298 K).

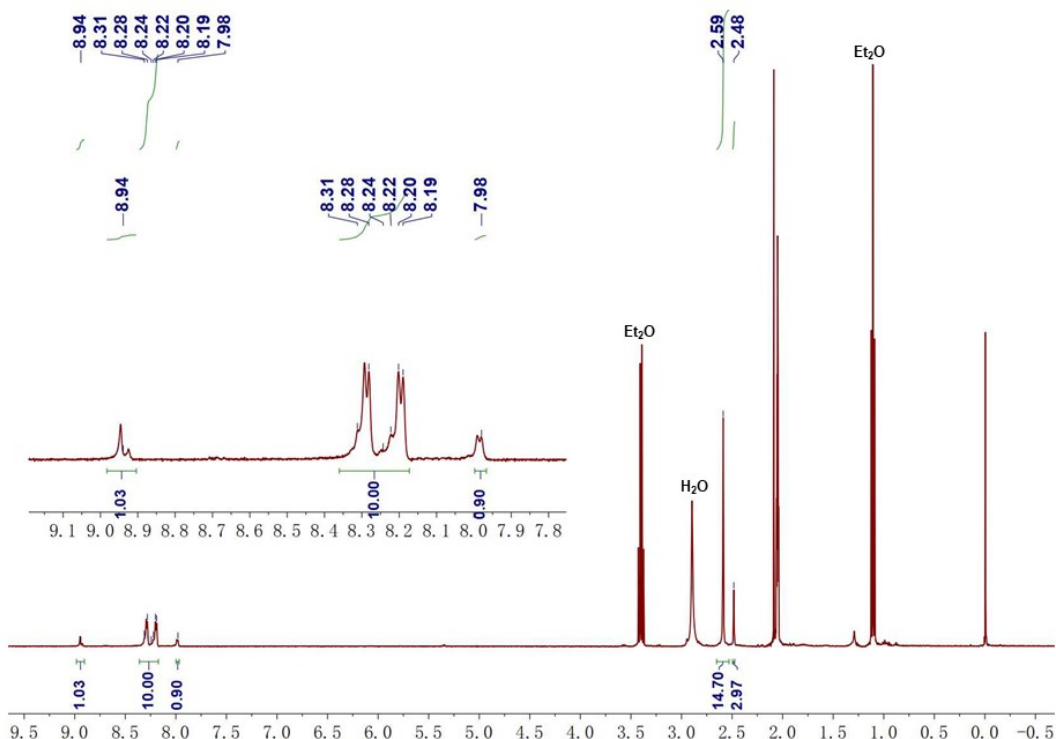


Figure S33. ¹H-NMR spectrum of complex $^{\text{Me}}\text{PyAg}_{13}$ (400 MHz, d_6 -acetone, 298 K).

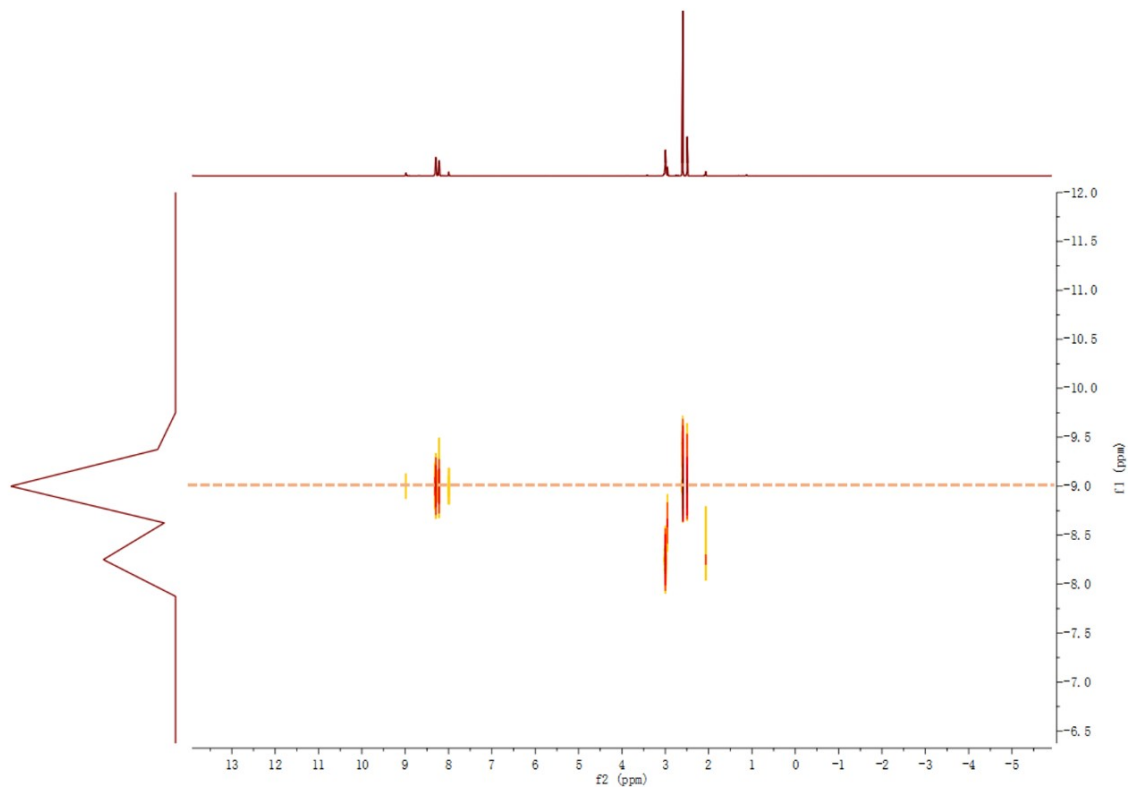


Figure S34. DOSY ^1H NMR spectrum (600 MHz, d_6 -acetone) of ${}^{\text{Me}}\text{PyAg}_{13}$.

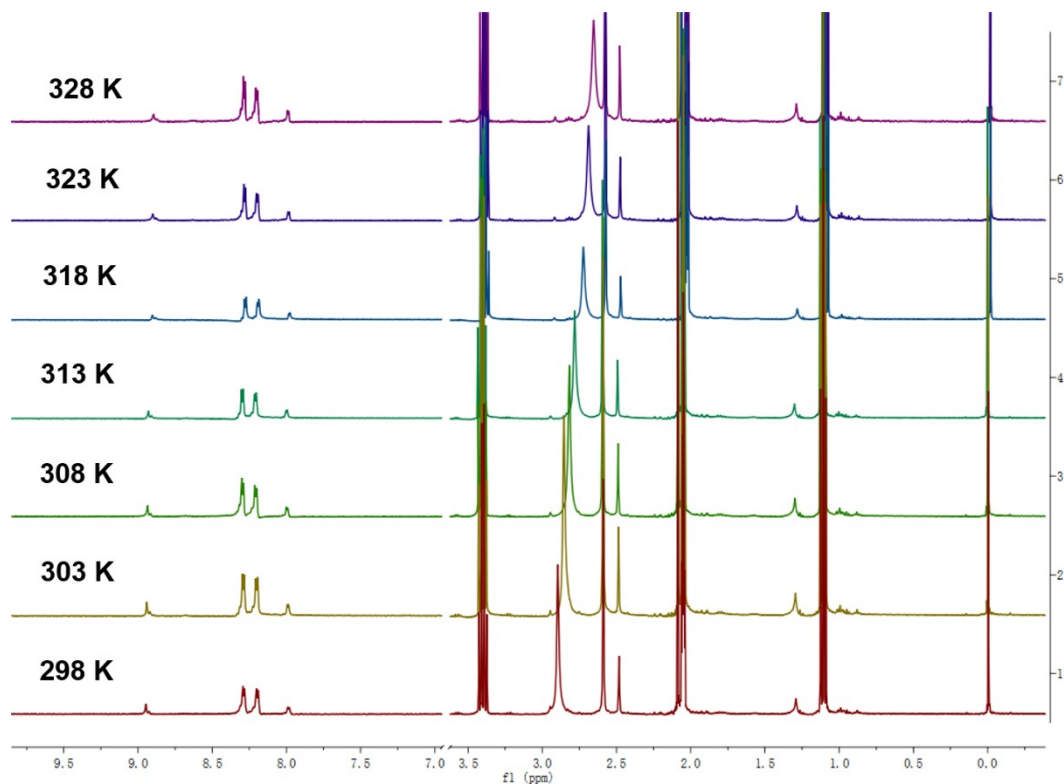


Figure S35. Variable temperature ^1H NMR spectra of ${}^{\text{Me}}\text{PyAg}_{13}$ (400 MHz, d_6 -acetone).

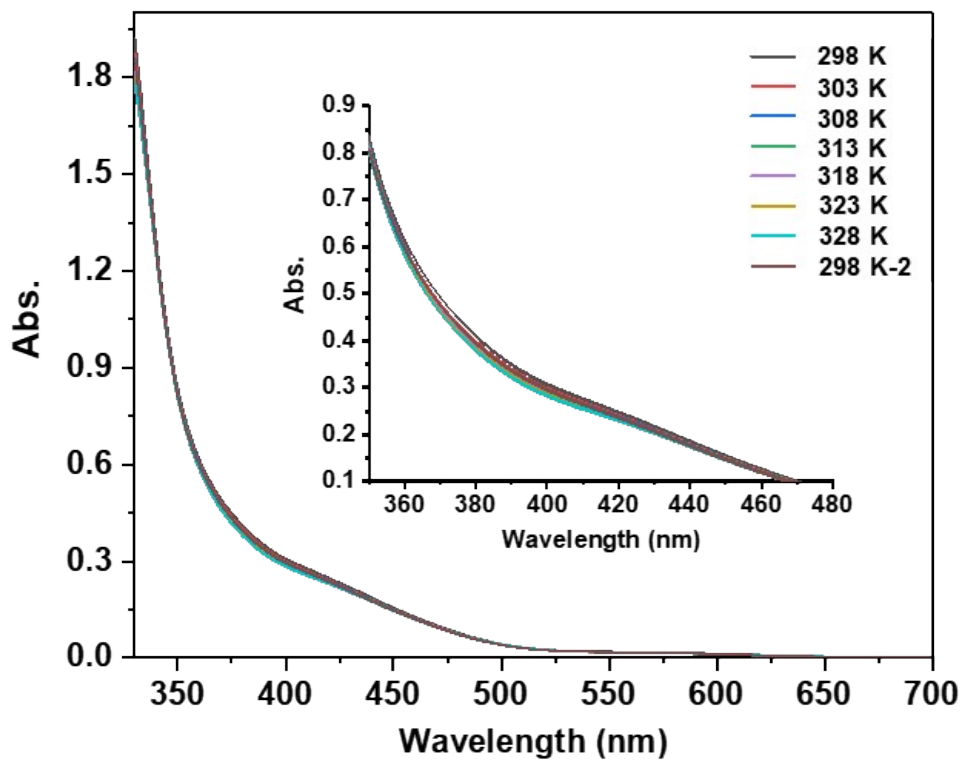


Figure S36. The variable temperature UV-vis spectra of MePyAg_{13} in acetone.

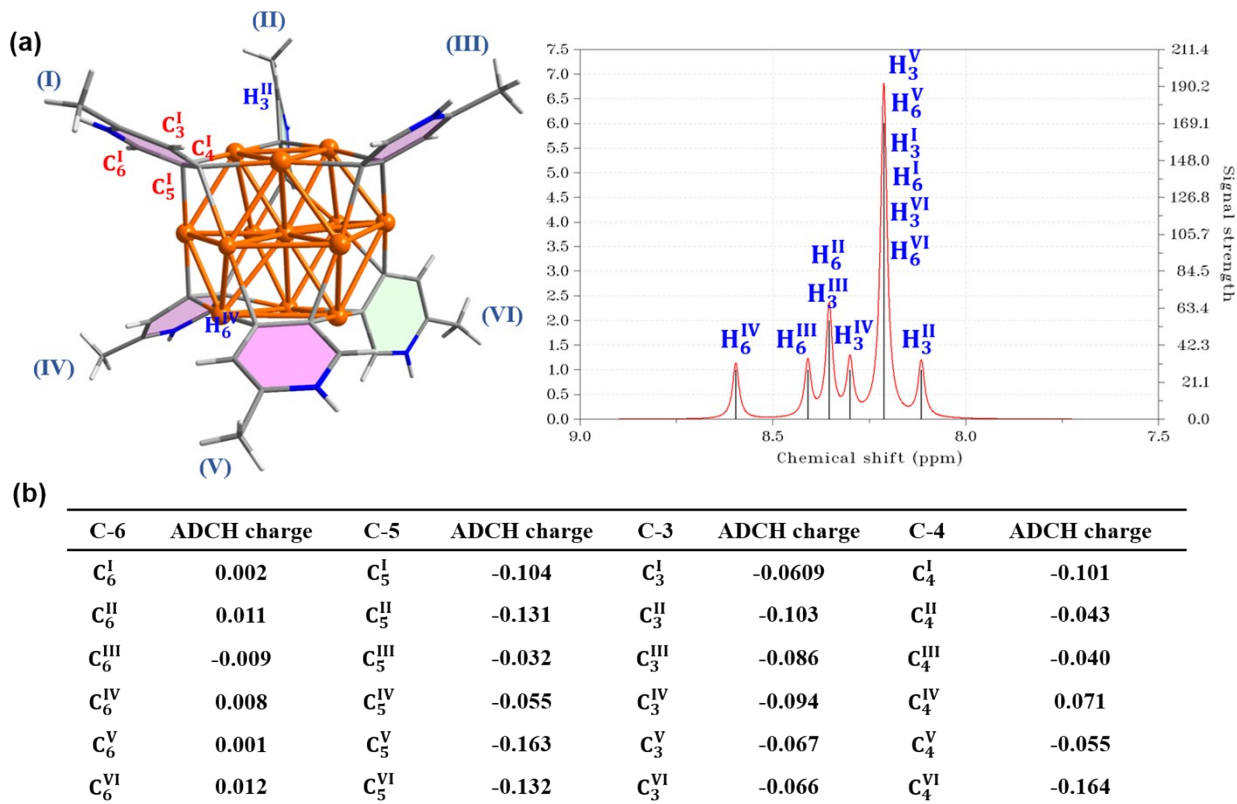


Figure S37. (a) Calculated NMR spectrum of MePyAg_{13} ; (b) Atomic dipole moment corrected Hirshfeld population (ADCH) of carbon atoms in MePyAg_{13} .

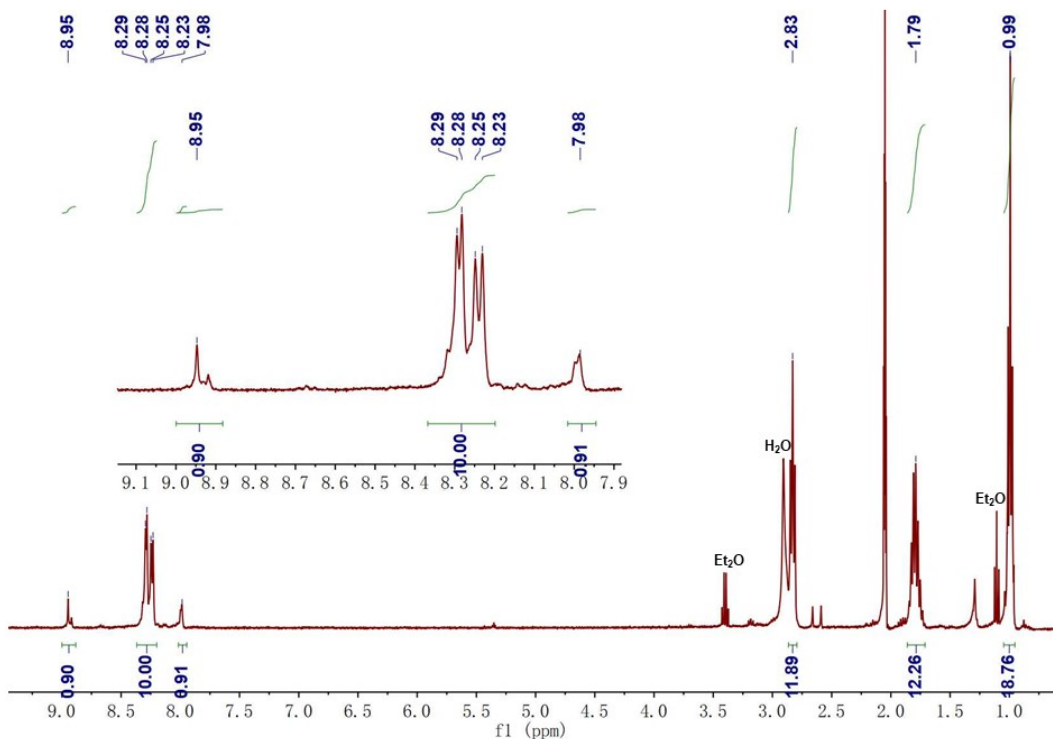


Figure S38. ^1H -NMR spectrum of complex $n\text{-PrPyAg}_{13}$ (400 MHz, d_6 -acetone, 298 K).

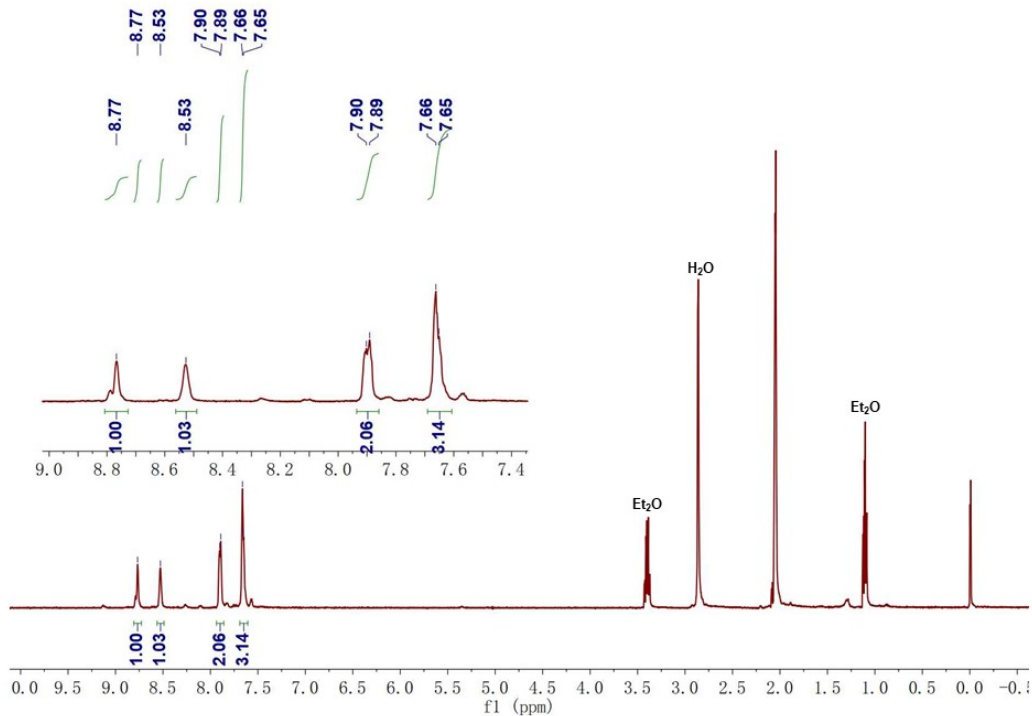


Figure S39. ^1H -NMR spectrum of complex PhPyAg_{13} (400 MHz, d_6 -acetone, 298 K).

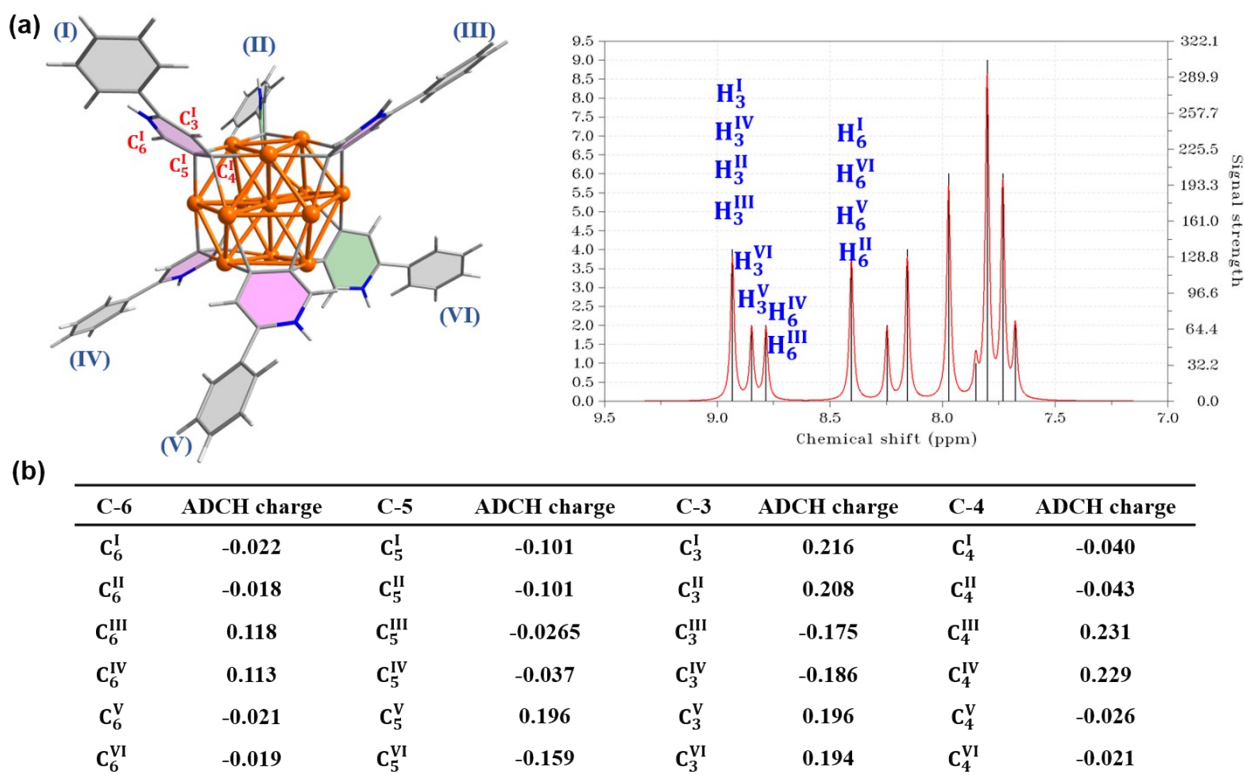


Figure S40. (a) Calculated NMR spectrum of $^{Ph}PyAg_{13}$; (b) Atomic dipole moment corrected Hirshfeld population (ADCH) of carbon atoms in $^{Ph}PyAg_{13}$.

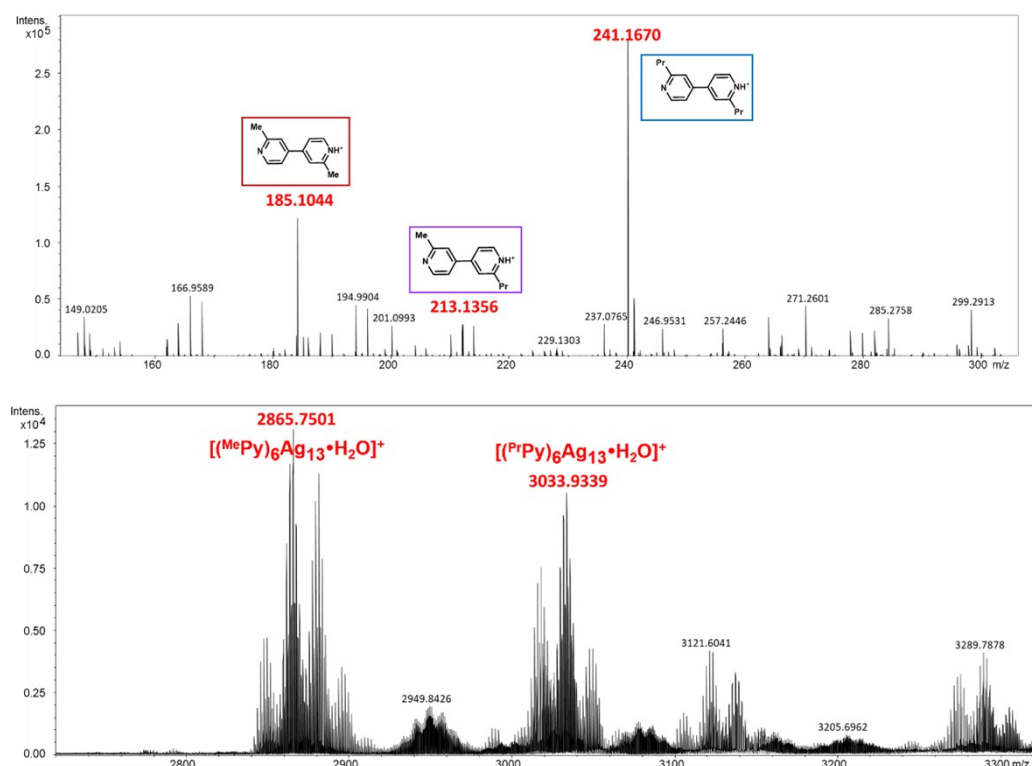


Figure S41. High resolution ESI-MS spectra monitoring on the simultaneously acidification of equivalent $^{Me}PyAg_{13}$ and $^{n-Pr}PyAg_{13}$ in acetone for 4 days.

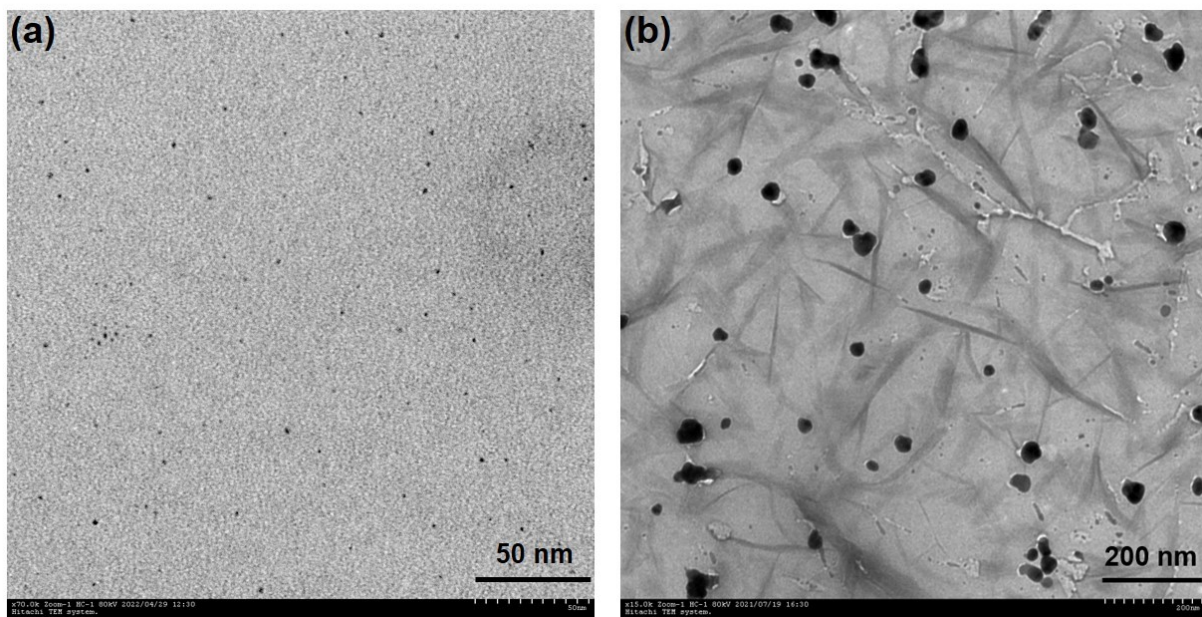


Figure S42. TEM images of (a) the individual atom-precise Ag_{13} NCs in acetone and (b) the solution sample derived from simultaneously acidification of equivalent $^{\text{Me}}\text{PyAg}_{13}$ and $n\text{-Pr}\text{PyAg}_{13}$ in acetone.

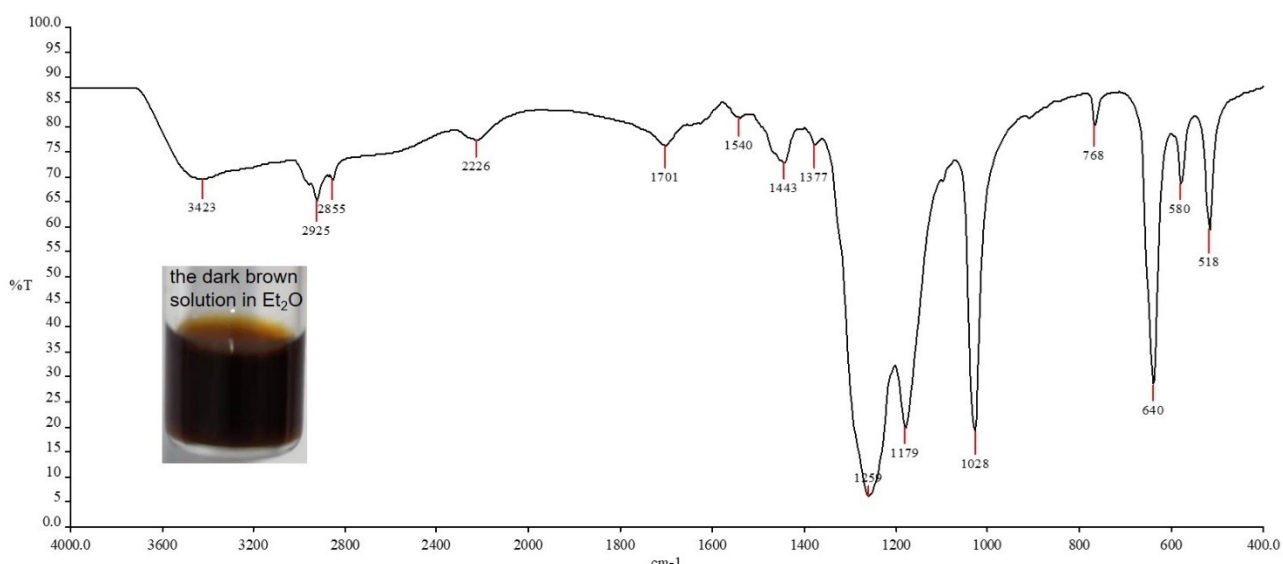


Figure S43. The infrared spectra of the solid in Et_2O after the reaction between $^{\text{Me}}\text{PyAg}_{13}$ cluster and $\text{CF}_3\text{SO}_3\text{H}$.

4. Supporting Tables

Table S1. Optimization of the reaction conditions.

^{Me} PyAg ₅ (mmol)	CF ₃ SO ₃ H (mmol)	Product	Yield
0.005	0.01	^{Me} PyAg ₅	75%
0.005	0.015	^{Me} PyAg ₅	61%
0.005	0.025	^{Me} PyAg ₅ , ^{Me} PyAg ₁₃	25%, 5%
0.005	0.035	^{Me} PyAg ₁₃	35%
0.005	0.05	^{Me} PyAg ₁₃	52%

Table S2. The Wiberg bond order of ^{Me}PyAg₁₃ based on Löwdin orthogonalized basis.

Bond	Wiberg bond order	Total	Bond	Wiberg bond order	Total
87(C)-3(Ag)	0.485	0.975	91(C)-2(Ag)	0.530	0.953
87(C)-2(Ag)	0.490		91(C)-10(Ag)	0.423	
53(C)-8(Ag)	0.435	0.898	47(C)-4(Ag)	0.551	0.893
53(C)-5(Ag)	0.464		47(C)-9(Ag)	0.341	
25(C)-3(Ag)	0.526	0.924	93(C)-10(Ag)	0.429	0.933
7(Ag)-25(C)	0.398		93(C)-13(Ag)	0.503	
24(C)-4(Ag)	0.553	0.907	49(C)-5(Ag)	0.446	0.908
24(C)-8(Ag)	0.355		49(C)-11(Ag)	0.462	
48(C)-8(Ag)	0.447	0.923	64(C)-9(Ag)	0.381	0.900
48(C)-7(Ag)	0.476		64(C)-13(Ag)	0.519	
55(C)-11(Ag)	0.435	0.942	50(C)-8(Ag)	0.394	0.921
55(C)-12(Ag)	0.507		50(C)-12(Ag)	0.527	

Bond (yellow)	Wiberg bond order	Bond (red)	Wiberg bond order	Bond (green)	Wiberg bond order
6(Ag)-1(Ag)	0.227	4(Ag)-9(Ag)	0.372	4(Ag)-2(Ag)	0.213
7(Ag)-1(Ag)	0.258	10(Ag)-2(Ag)	0.336	10(Ag)-9(Ag)	0.247
3(Ag)-1(Ag)	0.258	4(Ag)-8(Ag)	0.348	4(Ag)-3(Ag)	0.230
5(Ag)-1(Ag)	0.261	3(Ag)-7(Ag)	0.358	8(Ag)-7(Ag)	0.224
11(Ag)-1(Ag)	0.260	3(Ag)-2(Ag)	0.366	8(Ag)-3(Ag)	0.242
8(Ag)-1(Ag)	0.276	8(Ag)-4(Ag)	0.370	5(Ag)-2(Ag)	0.208
2(Ag)-1(Ag)	0.274	11(Ag)-5(Ag)	0.352	7(Ag)-12(Ag)	0.200
9(Ag)-1(Ag)	0.252	10(Ag)-13(Ag)	0.366	8(Ag)-11(Ag)	0.240
4(Ag)-1(Ag)	0.239	9(Ag)-13(Ag)	0.384	13(Ag)-11(Ag)	0.193
10(Ag)-1(Ag)	0.277	8(Ag)-12(Ag)	0.331	10(Ag)-5(Ag)	0.232
12(Ag)-1(Ag)	0.290	8(Ag)-7(Ag)	0.380	8(Ag)-9(Ag)	0.249
13(Ag)-1(Ag)	0.244	11(Ag)-12(Ag)	0.339	12(Ag)-13(Ag)	0.189

Table S3. The multi-center bond order (MCBO) of each CAg₂ species in ^{Mc}PyAg₁₃.

Bond	MCBO	Bond	MCBO	Bond	MCBO
3(Ag)-25(C)-7(Ag)	0.076	2(Ag)-91(C)-10(Ag)	0.091	6(Ag)-48(C)-7(Ag)	0.034
4(Ag)-24(C)-8(Ag)	0.030	4(Ag)-47(C)-9(Ag)	0.050	11(Ag)-49(C)-5(Ag)	0.013
3(Ag)-87(C)-2(Ag)	0.074	11(Ag)-55(C)-12(Ag)	0.050	9(Ag)-64(C)-13(Ag)	0.019
5(Ag)-53(C)-6(Ag)	0.048	10(Ag)-93(C)-13(Ag)	0.052	8(Ag)-50(C)-12(Ag)	0.071

Table S4. Topological and energetic properties of $\rho(r)$ calculated at the (3,-1) critical point in AIM analysis of ^{Mc}PyAg₁₃ (given in a.u.)

Bond	$\rho(r)$	$V(r)$	$\nabla^2\rho(r) \times 10^{-2}$	$G(r)$	$ V(r) /G(r)$	$E(r) \times 10^{-3}$	$E(r)/\rho(r)$
8(Ag)-1(Ag)	0.024	-0.018	5.710	0.016	1.119	-1.925	-0.082
7(Ag)-1(Ag)	0.029	-0.024	6.868	0.021	1.172	-3.575	-0.125
3(Ag)-1(Ag)	0.026	-0.021	6.396	0.019	1.143	-2.667	-0.103
5(Ag)-1(Ag)	0.029	-0.025	6.838	0.021	1.180	-3.759	-0.129
11(Ag)-1(Ag)	0.028	-0.024	6.817	0.020	1.161	-3.259	-0.117
6(Ag)-1(Ag)	0.032	-0.029	7.604	0.024	1.201	-4.792	-0.148
2(Ag)-1(Ag)	0.029	-0.025	6.835	0.021	1.181	-3.764	-0.129
9(Ag)-1(Ag)	0.028	-0.023	6.583	0.020	1.172	-3.407	-0.121
4(Ag)-1(Ag)	0.023	-0.017	5.462	0.016	1.122	-1.898	-0.081
10(Ag)-1(Ag)	0.032	-0.028	7.449	0.023	1.197	-4.568	-0.145
12(Ag)-1(Ag)	0.032	-0.029	7.964	0.024	1.187	-4.592	-0.143
13(Ag)-1(Ag)	0.025	-0.019	5.984	0.017	1.130	-2.244	-0.091
4(Ag)-9(Ag)	0.040	-0.040	10.380	0.033	1.215	-7.101	-0.177
8(Ag)-5(Ag)	0.042	-0.043	11.116	0.035	1.210	-7.408	-0.177
9(Ag)-13(Ag)	0.043	-0.043	10.968	0.035	1.226	-7.989	-0.186
8(Ag)-7(Ag)	0.043	-0.043	11.076	0.036	1.221	-7.833	-0.183
4(Ag)-2(Ag)	0.016	-0.012	4.447	0.011	1.020	-0.223	-0.014
10(Ag)-9(Ag)	0.024	-0.018	5.781	0.016	1.121	-1.997	-0.082
4(Ag)-3(Ag)	0.018	-0.013	4.880	0.013	1.046	-0.582	-0.033
8(Ag)-7(Ag)	0.021	-0.017	5.427	0.015	1.103	-1.558	-0.073
8(Ag)-3(Ag)	0.022	-0.016	5.270	0.014	1.088	-1.264	-0.058
5(Ag)-2(Ag)	0.018	-0.013	4.424	0.012	1.066	-0.777	-0.042
7(Ag)-12(Ag)	0.017	-0.012	4.349	0.011	1.035	-0.391	-0.023
8(Ag)-11(Ag)	0.022	-0.017	5.500	0.015	1.101	-1.546	-0.070
13(Ag)-11(Ag)	0.016	-0.011	4.176	0.011	1.023	-0.245	-0.016
10(Ag)-5(Ag)	0.022	-0.017	5.528	0.016	1.113	-1.756	-0.080
8(Ag)-9(Ag)	0.024	-0.019	5.983	0.017	1.131	-2.251	-0.092
12(Ag)-13(Ag)	0.015	-0.010	4.004	0.010	1.001	-0.011	-0.001

Bond	$\rho(r)$	$V(r)$	$\nabla^2\rho(r) \times 10^{-2}$	$G(r)$	$ V(r) /G(r)$	$E(r) \times 10^{-3}$	$E(r)/\rho(r)$
133(O)-43(H)	0.048	-0.041	14.972	0.039	1.050	-1.952	-0.041
61(H)-138(O)	0.005	-0.003	1.979	0.004	0.730	1.053	0.212
136(F)-61(H)	0.002	-0.001	0.810	0.001	0.489	0.684	0.441
41(O)-61(H)	0.009	-0.006	3.373	0.007	0.842	1.148	0.131
71(H)-122(O)	0.007	-0.005	2.717	0.006	0.840	0.938	0.127
35(O)-71(H)	0.007	-0.004	2.636	0.005	0.785	1.168	0.172
32(H)-122(O)	0.006	-0.004	2.421	0.005	0.793	1.039	0.166

63(O)-32(H)	0.006	-0.004	2.490	0.005	0.777	1.137	0.180
130(H)-116(F)	0.002	-0.001	1.147	0.002	0.601	0.817	0.385
83(F)-66(H)	0.004	-0.002	2.038	0.004	0.651	1.318	0.329
21(O)-66(H)	0.006	-0.004	2.604	0.005	0.776	1.192	0.184
52(H)-37(O)	0.005	-0.003	2.030	0.004	0.733	1.069	0.218
45(H)-88(O)	0.006	-0.004	2.452	0.005	0.785	1.084	0.174
67(O)-45(H)	0.007	-0.004	2.639	0.005	0.791	1.142	0.170

Table S5. Dihedral angles between the upper and lower Ag_3 planes and mean deviations of the central Ag_7 layer in ${}^{\text{Me}}\text{PyAg}_{13}$, ${}^{n\text{-Pr}}\text{PyAg}_{13}$, ${}^{\text{Ph}}\text{PyAg}_{13}$.

	${}^{\text{Me}}\text{PyAg}_{13}$	${}^{n\text{-Pr}}\text{PyAg}_{13}$	${}^{\text{Ph}}\text{PyAg}_{13}$
Dihedral angle between the upper and lower Ag_3 planes($^{\circ}$)	9.7	11.5	11.7
Mean deviation of the central Ag_7 layer (\AA)	0.094	0.125	0.104

Table S6. Diffusion coefficients, and the calculated and measured sizes of ${}^{\text{Me}}\text{PyAg}_{13}$ based on DOSY measurements.

Species	Diffusion coefficients / $\text{m}^2 \text{s}^{-1}$	Calculated diameter / \AA	Diameter in crystal structures / \AA
Major (8.28 and 8.19 ppm)	7.35×10^{-10}	18.75	17.55
Minor (8.94 and 7.98 ppm)	7.28×10^{-10}	18.98	--

Table S7. High resolution ESI-MS data for simultaneously acidification of equivalent ${}^{\text{Me}}\text{PyAg}_5$ and ${}^{n\text{-Pr}}\text{PyAg}_5$ in acetone.

Experimental	Theoretical	Chemical Formula	
2905.8671	2905.838	$\text{C}_{46}\text{H}_{44}\text{Ag}_{13}\text{F}_{18}\text{N}_6\text{O}_{18}\text{S}_6$	$({}^{\text{Me}}\text{Py})_4({}^{n\text{-Pr}}\text{Py})_2\text{Ag}_{13}^+$
2921.8655	2921.849	$\text{C}_{46}\text{H}_{46}\text{Ag}_{13}\text{F}_{18}\text{N}_6\text{O}_{19}\text{S}_6$	$({}^{\text{Me}}\text{Py})_4({}^{n\text{-Pr}}\text{Py})_2\text{Ag}_{13}\bullet\text{H}_2\text{O}^+$
2935.8762	2935.849	$\text{C}_{47}\text{H}_{46}\text{Ag}_{13}\text{F}_{18}\text{N}_6\text{O}_{19}\text{S}_6$	$({}^{\text{Me}}\text{Py})_5({}^{n\text{-Pr}}\text{Py})\text{Ag}_{13}\bullet\text{C}_3\text{H}_6\text{O}^+$
2949.8907	2949.881	$\text{C}_{48}\text{H}_{49}\text{Ag}_{13}\text{F}_{18}\text{N}_6\text{O}_{19}\text{S}_6$	$({}^{\text{Me}}\text{Py})_3({}^{n\text{-Pr}}\text{Py})_3\text{Ag}_{13}\bullet\text{H}_2\text{O}^+$
2963.9008	2963.880	$\text{C}_{49}\text{H}_{50}\text{Ag}_{13}\text{F}_{18}\text{N}_6\text{O}_{19}\text{S}_6$	$({}^{\text{Me}}\text{Py})_4({}^{n\text{-Pr}}\text{Py})_2\text{Ag}_{13}\bullet\text{C}_3\text{H}_6\text{O}^+$
2977.9159	2977.912	$\text{C}_{50}\text{H}_{54}\text{Ag}_{13}\text{F}_{18}\text{N}_6\text{O}_{19}\text{S}_6$	$({}^{\text{Me}}\text{Py})_2({}^{n\text{-Pr}}\text{Py})_4\text{Ag}_{13}\bullet\text{H}_2\text{O}^+$
2991.9250	2991.911	$\text{C}_{51}\text{H}_{54}\text{Ag}_{13}\text{F}_{18}\text{N}_6\text{O}_{19}\text{S}_6$	$({}^{\text{Me}}\text{Py})_3({}^{n\text{-Pr}}\text{Py})_3\text{Ag}_{13}\bullet\text{C}_3\text{H}_6\text{O}^+$
3005.9418	3005.943	$\text{C}_{52}\text{H}_{58}\text{Ag}_{13}\text{F}_{18}\text{N}_6\text{O}_{19}\text{S}_6$	$({}^{\text{Me}}\text{Py})({}^{n\text{-Pr}}\text{Py})_5\text{Ag}_{13}\bullet\text{H}_2\text{O}^+$

5. References

1. M. J. Frisch, et al. Gaussian 09, Revision D.01 (Gaussian, Inc., Wallingford, CT, 2013).
2. F. Neese, F. Wennmohs, U. Becker and C. Riplinger. *J. Chem. Phys.*, 2020, **152**, 224108.
3. A. Schäfer, C. Huber and R. Ahlrichs. *J. Chem. Phys.*, 1994, **100**, 5829.
4. J. P. Perdew. *Phys. Rev. B*, 1986, **33**, 8822.
5. A. V. Marenich, C. J. Cramer and D. G. Truhlar. *J. Phys. Chem. B*, 2009, **113**, 6378.
6. (a) M. W. Lodewyk, M. R. Siebert and D. J. Tantillo. *Chem. Rev.*, 2012, **112**, 1839; (b) P. R. Rablen, S. A. Pearlman and J. Finkbiner. *J. Phys. Chem. A*, 1999, **103**, 7357; (c) R. Jain, T. Bally and P. R. Rablen. *J. Org. Chem.*, 2009, **74**, 4017; (d) T. Bally and P. R. Rablen. *J. Org. Chem.*, 2011, **76**, 4818.
7. P. J. Stephens, F. J. Devlin, C. F. Chabalowski and M. J. Frisch. *J. Phys. Chem.*, 1994, **98**, 11623.
8. G. A. Petersson, et al. *J. Chem. Phys.*, 1988, **89**, 2193.
9. (a) M. Dolg, U. Wedig, H. Stoll and H. Preuss. *J. Chem. Phys.*, 1987, **86**, 866; (b) D. Andrae, U. Häußermann, M. Dolg, H. Stoll and H. Preuß. *Theoret. Chim. Acta*, 1990, **77**, 123.
10. T. Lu and F. Chen, *J. Comput. Chem.*, 2012, **33**, 580.
11. (a) W. R. Wadt and P. J. Hay. *J. Chem. Phys.*, 1985, **82**, 284; (b) P. J. Hay and W. R. Wadt. *J. Chem. Phys.*, 1985, **82**, 27; (c) P. J. Hay and W. R. Wadt. *J. Chem. Phys.*, 1985, **82**, 299; (d) T. H Jr. Dunning, P. J. Hay and H. F III. Schaefer. *Theory*. (Plenum Press: New York, 1977).
12. W. Humphrey, A. Dalke and K. Schulten, *J. Molec. Graphics*, 1996, **14.1**, 33.
13. G. M. Sheldrick. *Acta Crystallogr. Sect. A*, 2008, **64**, 112.
14. (a) P. van der Sluis and A. L. Spek. *Acta Crystallogr. Sect. A*, 1990, **46**, 194; (b) A. Spek. *J. Appl. Crystallogr.*, 2003, **36**, 7.
15. J. L. Atwood and L. J. Barbour. *Cryst. Growth Des.*, 2003, **3**, 3.